Neurobiology of Disease 127 (2019) 193–209

Contents lists available at ScienceDirect

Neurobiology of Disease

journal homepage: www.elsevier.com/locate/ynbdi

Genetic suppression of IKK2/NF-κB in astrocytes inhibits neuroinflammation and reduces neuronal loss in the MPTP-Probenecid model of Parkinson's disease

Kelly S. Kirkley[a], Katriana A. Popichak[a], Sean L. Hammond[a], Cecilia Davies[a], Lindsay Hunt[a], Ronald B. Tjalkens[a,b,*]

[a] Department of Environmental and Radiological Health Sciences, Colorado State University, Fort Collins, CO, USA 80523
[b] Program in Molecular, Cellular and Integrative Neuroscience, Colorado State University, Fort Collins, CO, USA 80523

ARTICLE INFO

Keywords:
Neuroinflammation
NFκB
Astrocytes
MPTP
IKK2
Transgenic models

ABSTRACT

Neuroinflammatory activation of glia is considered a pathological hallmark of Parkinson's disease (PD) and is seen in both human PD patients and in animal models of PD; however, the relative contributions of these cell types, especially astrocytes, to the progression of disease is not fully understood. The transcription factor, nuclear factor kappa B (NFκB), is an important regulator of inflammatory gene expression in glia and is activated by multiple cellular stress signals through the kinase complex, IKK2. We sought to determine the role of NFκB in modulating inflammatory activation of astrocytes in a model of PD by generating a conditional knockout mouse (*hGfapcre/Ikbk2$^{F/F}$*) in which IKK2 is specifically deleted in astrocytes. Measurements of IKK2 revealed a 70% deletion rate of IKK2 within astrocytes, as compared to littermate controls (*Ikbk2$^{F/F}$*). Use of this mouse in a subacute, progressive model of PD through exposure to 1-methyl-4-phenyl-1,2,3,6-tetrahydropyridine and probenecid (MPTPp) revealed significant protection in exposed mice to direct and progressive loss of dopaminergic neurons in the substantia nigra (SN). *hGfapcre/Ikbk2$^{F/F}$* mice were also protected against MPTPp-induced loss in motor activity, loss of striatal proteins, and genomic alterations in nigral NFκB gene expression, but were not protected from loss of striatal catecholamines. Neuroprotection in *hGfapcre/Ikbk2$^{F/F}$* mice was associated with inhibition of MPTPp-induced astrocytic expression of inflammatory genes and protection against nitrosative stress and apoptosis in neurons. These data indicate that deletion of IKK2 within astrocytes is neuroprotective in the MPTPp model of PD and suggests that reactive astrocytes directly contribute the potentiation of dopaminergic pathology.

1. Introduction

Activation of glial cells is implicated in the progression of neuronal loss in neurodegenerative disorders such as Parkinson's disease (PD) through the upregulation and release of pro-inflammatory and pro-oxidant factors that exert toxic effects on surrounding neurons (Hirsch and Hunot, 2009). Neuroinflammation is seen in both human patients and in animal models of PD, characterized by the presence of reactive astrocytes and microglia in affected brain regions that closely associate with protein aggregates (Damier et al., 1993; Nagatsu and Sawada, 2005; Ouchi et al., 2009). Several lines of evidence point to reactive glia being important participants in disease pathology, because upregulation of glial-derived factors such as tumor necrosis factor alpha (TNF) and inducible nitric oxide synthase 2 (NOS2) occurs prior to loss of dopaminergic neurons (Sugama et al., 2003; Hirsch and Hunot, 2009; Saijo et al., 2009; Miller et al., 2011) and alterations in familial PD genes can affect production of inflammatory cytokines (Dzamko et al., 2015). Experimental models in which these and other inflammatory factors are genetically or pharmacologically inhibited markedly protect against neurodegeneration (Dehmer et al., 2000, 2003; McCarty, 2006; Mondal et al., 2012). Yet, these studies have focused primarily on limiting microglia responses due to their early activation in the disease

Abbreviations: Dopamine Transporter, DAT); Glial Fibrillary Acidic Protein, GFAP); Ionized Binding Adaptor protein-1, IBA-1); Inducible Nitric Oxide Synthase, iNOS/NOS2); Inhibitory kappa alpha kinase beta, IKK2); Nuclear Factor kappa Beta, NFκB); Parkinson's Disease, PD); Striatum, ST); Substantia Nigra, SN); Tumor Necrosis Factor alpha, TNF); Tyrosine Hydroxylase, TH); Vesicular Monoamine Transporter, VMAT)

* Corresponding author at: Department of Environmental and Radiological Health Sciences, College of Veterinary Medicine and Biomedical Sciences, Colorado State University, 1680 Campus Delivery, Fort Collins, CO 80523-1680, USA.
E-mail address: Ron.Tjalkens@colostate.edu (R.B. Tjalkens).

https://doi.org/10.1016/j.nbd.2019.02.020
Received 2 November 2018; Received in revised form 20 December 2018; Accepted 22 February 2019
Available online 25 February 2019
0969-9961/

(Hirsch and Hunot, 2009), yielding hopeful targets for drug development that ultimately fail in clinical trials (Cheng et al., 2015). Additionally, although gliosis is associated with neuronal injury in PD (McCarty, 2006; Chen et al., 2009), glial responses can also be neuroprotective. In astrocytes this is linked with an A1 (neurotoxic) versus A2 (neuroprotective) phenotype (Frank-Cannon et al., 2009; Neal and Richardson, 2018; Liddelow et al., 2017), revealing time- and phenotype-dependent mechanisms in modulating neuronal function and survival.

Inflammatory signaling through the canonical (NFκB) pathway involves activation of inhibitory kappa alpha kinase beta (IKKβ/IKK2) and subsequent translocation of p65/p50 dimers to the nucleus that stimulate inflammatory gene expression through binding to *cis*-acting promoter elements (Karin, 1999; Bonizzi and Karin, 2004; Karin, 2005), which is critical for production of inflammatory mediators in glial cells (Glass et al., 2010). Activation of NFκB is directly associated with PD, as noted studies describe upregulation and nuclear translocation of NFκB/p65 in both neurons (Hunot et al., 1997) and glia of the PD brain (Ghosh et al., 2007) and in experimental animal models (Saijo et al., 2009). Studies have demonstrated that globally suppressing NFκB can be protective in neurotoxin-based models of PD (Dehmer et al., 2003; Ghosh et al., 2007; Saijo et al., 2009; Mondal et al., 2012; De Miranda et al., 2013) but these studies do not ascertain the specific cellular protective mechanisms and are difficult to translate to clinical applications due to detrimental effects from complete functional loss of NFκB (Grilli and Memo, 1999; Herrmann et al., 2005). Additionally, neuronal NFκB activation appears to protect neurons against degeneration (Mettang et al., 2018), whereas excess activation NFκB in glia promotes neurodegeneration (Mattson and Camandola, 2001; Brambilla et al., 2009; Zhang et al., 2017).

Previous studies in our laboratory utilizing a transgenic reporter mouse expressing green fluorescent protein under the control of NFκB enhancer elements reported activation of the pathway in astrocytes prior to an overt loss of dopaminergic neurons in the substantia nigra pars compacta (SNpc; Miller et al., 2011). Other neurodegenerative models including multiple sclerosis, traumatic spinal cord injury, and Huntington's disease have also shown that selective deletion of the NFκB pathway to be neuroprotective (Brambilla, 2005; van Loo et al., 2006; Brambilla et al., 2009) while constitutive activation to lead to high levels of basal inflammation (Oeckl et al., 2012). Based on these previous studies, we postulated that cell-specific inhibition of inflammatory NFκB signaling in astrocytes would suppress a reactive phenotype and protect dopaminergic neurons in the MPTPp model of PD. As the phosphorylation of the IκB inhibitor complex by IKKβ/IKK2 is an important regulatory step in the classical inflammatory pathway of NFκB (Karin, 1999), we sought to test this hypothesis by utilizing Cre-loxP technology to delete IKKβ/IKK2 selectively in astrocytes to determine the role of this signaling factor in injury to dopaminergic neurons.

2. Materials and methods

2.1. Animals and genotyping

Astrocyte-specific *Ikbk2*-deficient mice (*hGfapcre/Ikbk2*$^{F/F}$) were generated by breeding *Ikbk2*-floxed mice (Li et al., 2003); C57Bl/6 background; provided by Dr. Michael Karin at University of California San Diego) with *hGfapcre* transgenic mice (Zhuo et al., 2001); FVB-Tg (GFAP-CRE)25Mes/J; FVB background; Jackson Laboratories, Bar Harbor, ME) expressing Cre under the control of the human glial fibrillary acidic protein (GFAP) promoter. Mice were bred to homozygosity for the floxed-*Ikbk2* allele and both male and female littermates from the 4th generation aged to 5 months were utilized in expression and treatment studies. The majority of animals were used in studies by 5 months of age to avoid the development of spontaneous inflammatory and neoplastic skin lesions associated with this genotype during aging, as we recently reported (Kirkley et al., 2017a). Littermates lacking *hGfapcre* (known as *Ikbk2*$^{F/F}$) were utilized as controls.

PCR genotyping on ear tags was performed using the primers 5'-GTC ATT TCC ACA GCC CTG TGA-3′ and 5'-CCT TGT CCT ATA GAA GCA CAA C-3′, that amplifies both the *Ikbk2*$^{+}$ (220-bp) and *Ikbk2*^{F} (310-bp) alleles and primers 5'-ACT CCT TCA TAA AGC CCT CG-3′ and 5'-ATC ACT CGT TGC ATC GAC CG-3′, to amplify the *hGfapcre* allele (190-bp). Animals were housed in microisolator cages (2–3 animals per cage), kept on a 12-h light/dark cycle, and had access to both chow and water ad libitum. All procedures were performed in accordance with National Institutes of Health guidelines for the care and use of laboratory animals and with the approval by the Institutional Animal Care and Use Committee (IACUC) of Colorado State University.

2.2. Primary glial and neuronal cultures

Mixed glial cultures from whole brain (excluding cerebellum and brain stem) of postnatal day 1 (neonatal) and 3-month old (adult) *Ikbk2*$^{F/F}$ and *hGfapcre/Ikbk2*$^{F/F}$ mice were isolated using a modification of a previously described method (Aschner and Kimelberg, 1991; Carbone et al., 2008; Moreno et al., 2008). Briefly, mice were euthanized by decapitation under isoflurane anesthesia and whole brains were rapidly dissected out and placed into ice-cold minimum essential medium with L-glutamine (MEM; Gibco). Meninges were removed, and tissues completely digested with dispase (1.5 U/ml) with each animal extracted separately. Dissociated cells from individual animals were plated onto 100-mm tissue culture plates and kept in MEM supplemented with 10% heat-inactivated FBS (Sigma) and penicillin (0.002 mg/ml), streptomycin (0.002 mg/ml), and neomycin (0.001 mg/ml) antibiotic mixture (PSN). Media was changed every 4–5 days and cells were maintained at 37 °C and 5% CO2 in humidified chambers until confluency was reached (~14–18 days). Microglia were purified from astrocytes via column-free magnetic separation using the EasySep mouse CD11b positive selection kit (Stemcell Technologies, Vancouver, Canada) according to manufacturer instructions and as described (Gordon et al., 2011; Kirkley et al., 2017b) and determined to be 97% pure via flow cytometry.

Primary striatal neurons were extracted in a similar fashion as the mixed glial cultures except performed in neurobasal medium. Primary neuronal cultures were seeded onto poly(L-lysine)-coated 22 mm glass coverslips at 4×10^5 cells/well and maintained in neurobasal media supplemented with 2 mM L-glutamine, B27 supplement, and PSN antibiotic mixture (Gibco, Waltham, MA). Neuronal culture media was changed every 2 days with purity ascertained via cell morphology and immunolabeling with the neuron-specific marker microtubule-associated factor 2 (MAP2).

2.3. Flow cytometry

The percent of glia in astrocyte cultures were determined by immunophenotyping using direct labeling with anti-GLAST-PE (Miltenyi Biotec, San Diego, CA), anti-Cd11b-FITC (BD Biosciences, San Jose, CA) followed by flow cytometric analysis as described (Kirkley et al., 2017). Briefly, purified cells were counted using a Bio-Rad TC10 automated cell counter, and 1×10^6 cells/ml were resuspended in 100 µl of incubation buffer (PBS with 0.05% bovine serum albumin). Purified cells were labeled using the mouse anti-GLAST-PE (20 µg/ml) and mouse anti-CD11b-FITC (10 µg/ml) at room temperature for 1 h. After labeling, the cells were washed twice in incubation buffer and resuspended at a final volume of 500 µl of PBS and stored at 37 °C until analysis. Flow cytometry was performed on a Beckman Coulter CyAn ADP flow cytometer operated with Summit software for data collection at Colorado State University's Flow Cytometry Core Facility. All further data analysis was done utilizing FlowJo software (version 10.1; FlowJo, Ashland, OR).

2.4. Evaluation of genomic deletion of *Ikbk2*$^{F/F}$ via qPCR

Genomic DNA was isolated from neonatal and adult astrocyte cultures and neonatal microglia and striatal neuronal cultures utilizing a DNeasy kit (Qiagen, Valencia, CA) with purity and concentration confirmed using a Nanodrop ND-1000 spectrophotometer (NanoDrop Technologies, Wilmington, DE). 100 ng of DNA was mixed with Sybrgreen (Bio-Rad, Hercules, CA) and primers (10 μM) 5′-AAG ATG GGC AAA CTG TGA TGT G-3′ and 5'-CAT ACA GGC ATC CTG CAG AAC A-3′ to amplify the *Ikbk2*^{F} allele or 5′-ATG GCC TTG CAT GAG GAT ACA CCA-3′ and 5′-GAG TCT CAG TCT TCA ACT CCC TGT-3′ to amplify the *Nos2* promoter which was utilized as a control. Percent expression of *Ikbk2*^{F} in astrocytes, microglia, and neurons from *hGfapcre/Ikbk2*$^{F/F}$ mice was determined based on a comparison of *Ikbk2*^{F} signal from *Ikbk2*$^{F/F}$ littermate controls, defined at 100%, after normalization to *Nos2* promoter signal.

2.5. Measurement of IKK2 via Western blot

Purified neonatal astrocyte cultures from *Ikbk2*$^{F/F}$ and *hGfapcre/Ikbk2*$^{F/F}$ and mice were lysed using a RIPA lysis buffer supplemented with complete protease inhibitor (Roche, Indianapolis, IN). Protein was quantified using a BCA Assay (Pierce, Rockford, IL) and 50 μg of protein was separated using gel electrophoresis in a 10% SDS polyacrylamide gel followed by a wet transfer to a polyvinylidene fluoride membrane (Pall Corporation, Pensacola, FL). Membranes were blocked in 5% non-fat dry milk in Tris-buffered saline containing 0.2% Tween-20 then incubated with primary rabbit anti-IKK2 (1:500; Cell Signaling, Danvers, MA) overnight followed by incubation in horseradish peroxidase-conjugated secondary antibody (1:5000, Santa Cruz, Dallas, TX) for one hour. Chemiluminescent detection was performed and analyzed using the ChemiDoc XRX imaging system (Bio-Rad). Membranes were reprobed with β-actin as a control with all densitometric analysis normalized to β-actin signal using Fiji software.

2.6. Immunofluorescence of IKK2

Purified astrocytes, microglia, and striatal neurons from *Ikbk2*$^{F/F}$ and *hGfapcre/Ikbk2*$^{F/F}$ mice were plated at a density of 1×10^4 cells on 12 mm poly-D-lysine coated glass coverslips and allowed to adhere for 48 h. Cells were fixed using methanol, washed in PBS, and then blocked in 1% bovine serum albumin (w/v) in PBS for one hour. Cells were incubated overnight at 4 °C in primary antibodies for IKK2 (1:50; Imgenex, San Diego, CA) and for cell-specific markers GFAP (1:500; Sigma, St. Louis, MO), ionized binding adaptor protein-1 (IBA1; 1:250; Wako, Osaka, Japan), or MAP2 (1:100; Abcam, Cambridge, MA). After rinsing in PBS, cells were incubated in for one hour at room temperature in AlexaFluor-488 (IKK2) and AlexaFluor-647 (cell markers) conjugated secondary antibodies (1:500; Invitrogen, Carlsbad, CA) and then mounted in medium containing 4′,6-diamidino-2-phenylindole dihydrochloride (DAPI) to detect cell nuclei.

In vivo assessment of IKK2 was performed on free-floating 40 μm brain sections obtained from the SN of *Ikbk2*$^{F/F}$ and *hGfapcre/Ikbk2*$^{F/F}$ mice (procedure detailed below) using primary antibodies for IKK2 (1:50; Imgenex) and MAP2 (1:100; Abcam) and Alexafluor-488 and Alexa-Fluor-647 conjugated secondary antibodies (1:500; Invitrogen). Sections were mounted in medium containing DAPI. Images were acquired using a 40× air plan apochromatic objectives on a Zeiss Axiovert 200 M inverted fluorescence microscope (Carl Zeiss, Inc., Thornwood, NY) equipped with a Hamamatsu ORCA-ER-cooled charge-coupled device camera (Hamamatsu Photonics, Hamamatsu City, Japan). Mean fluorescence intensity of IKK2, reported with a subtraction of mean background fluorescence, was determined by utilizing Slidebook software (Intelligent Imaging Innovations Inc., Denver, CO) with 10–15 individual fields examined per animal with at least 3 animals utilized per genotype.

2.7. MPTP treatment protocol

Ikbk2$^{F/F}$ and *hGfapcre/Ikbk2*$^{F/F}$ male and female littermates aged to 5 months were divided between treatment groups and then exposed to a subacute PD lesioning model utilizing 1-methyl-4-phenyl-1,2,3,6-tetrahydropyridine/probenecid (MPTPp) as described previously (Miller et al., 2011; De Miranda et al., 2013). In brief, mice were injected every other day with probenecid (250 mg/kg i.p. prepared in 5% sodium bicarbonate; Sigma) and with saline or MPTP (20 mg/kg s.c. prepared in saline as a free base, Sigma) for 7 days receiving a total of 4 injections. Mice were euthanized under deep isoflurane anesthesia at either 7 days (MPTPp7d) or 14 days (MPTPp14d) after their initial injection (Fig. 3A). For all groups, a minimum of 7 mice was utilized per parameter (stereology versus neurochemistry) with a minimum of 10 mice used for neurobehavioral data. All procedures were performed under an approved IACUC protocol in accordance with NIH policy for the care and use of laboratory species to minimize pain and discomfort.

2.8. Tissue processing and sectioning

At day 7 and 14, mice were euthanized, and tissues obtained as reported previously (Miller et al., 2011). Briefly, animals were terminated under isoflurane anesthesia and transcardially perfused with 20 mM cacodylate-phosphate buffered saline (cPBS) containing 10 U/ml heparin, followed by 4% paraformaldehyde in cPBS. Brains were carefully removed from the skull and placed within 4% formaldehyde in cPBS overnight then cryoprotected in 15% sucrose (w/v cPBS) then 30% sucrose (w/v cPBS). Brains were stored in 30% sucrose at 4 °C until sectioning. Coronal 40 μm sections through the entire length of the striatum (ST) and substantia nigra (SN) were collected using a freezing sliding microtome (Microm HM450; Thermoscientific, Waltham, MA). Sections were stored free floating at −20 °C in cryoprotectant (30% w/v sucrose, 30% v/v ethylene glycol; 0.05 M phosphate buffer) until staining.

2.9. Stereological counts of tyrosine hydroxylase (TH) positive neurons

Stereological assessment of TH-positive dopaminergic neurons within the SN were done perfomed in "Miller et al., 2011." In brief, free-floating serial sections were obtained by systematic sampling of every third tissue from sections encompassing the entire length of the SNpc and immunolabeled using primary rabbit anti-TH antibody (1:500 overnight, Chemicon, Temecula, CA) and AlexaFluor-555 conjugated secondary antibody (1:500 for 3 h; Invitrogen). Slides were mounted in DAPI containing medium and stored at 4 °C until imaging.

Slides were imaged using a 40× air plan apochromatic objective on a Zeiss Axiovert 200 M inverted fluorescence microscope (Carl Zeiss) with stereological counts of TH-positive cells performed using Slidebook software (v5.0, Intelligent Imaging Innovations, Denver, CO). The boundary of the SNpc was determined using 10× magnification montaging and numbers of TH-positive cells determined via assessment of uniform (40×) randomly placed counting frames (100 μm × 100 μm) using an optical dissector of 30 μm with 5 μm upper and lower guard zones. Representative montage images were generated for each treatment group with use of BX51 microscope (Olympus, Center Valley, PA, USA) equipped with a Hamamatsu ORCA-Flash4.0 digital CMOS camera, ProScan III stage controller (Prior, Rockland, MA USA) and CellSens Dimension software (version 1.12, Olympus, Center Valley, PA, USA). Representative images were processed using Fiji (National Institutes of Health freeware) with shade correction, standard background subtraction, and contrast enhancement. Original hues were altered when indicated to limit the use of red-green combinations and for consistency.

2.10. Behavioral assessment

Open field activity parameters were assessed using the Versamax behavior chambers with an infrared beam grid detection array (Accuscan Instruments, Inc., Columbus, OH). Mice were monitored for 10 min under low ambient light in the presence of white noise. Stride length was assessed via video recording mice freely walking across a plexiglass track (5 cm × 1 m) with 3 recordings obtained per mouse per assessment. Animals were pre-conditioned one day prior to their first treatment and then assessed at day 0 (first day of treatment) to establish a baseline, day 7, and day 14. Several behavioral parameters were collected and analyzed using Versadat Software (Accuscan Instruments, Inc.) including total distance traveled, number of movements, time spent moving, time spent in the margin, and the number of rearing movements. Stride length was calculated using the Tracker Video Modeling software (Tracker v.4.85 for MacOS X). These parameters have been previously shown to assess basal ganglia function (Liu et al., 2006; Moreno et al., 2009; Miller et al., 2011; Streifel et al., 2012) and were reported as a change from baseline (day 0) assessment.

2.11. HPLC analysis of striatal dopamine and metabolites

Mice were terminated at day 7 and day 14 under deep isoflurane anesthesia and quickly decapitated followed by rapid removal of the ST using a brain matrix block for reference. The tissue was flash-frozen in liquid nitrogen and stored at −80 °C until analysis. Samples were coded for unbiased analysis and sent to the Neurochemistry Core Laboratory at Vanderbilt University's Center for Molecular Neuroscience Research (Nashville, TN). High-Performance Liquid Chromatography with electrochemical detection was used to determine the concentrations of dopamine (DA) and dopamine-related metabolites 3,4-dihydroxyphenylacetic acid (DOPAC), and homovanillic acid (HVA) in the striatum of control and MPTPp treated mice as detailed in (Perez and Palmiter, 2005).

2.12. Western blot analysis of striatal proteins

Flash-frozen striatal tissue from *Ikbk2*$^{F/F}$ and *hGfapcre/Ikbk2*$^{F/F}$ mice was collected at day 7 and day 14, flash frozen in liquid nitrogen and stored at −80 °C until homogenized using a glass pestle and grinder followed by low power sonication in RIPA lysis buffer supplemented with a complete protease inhibitor. Protein was quantified using a BCA Assay (Pierce, Rockford, IL) and 20 μg of protein was separated using gel electrophoresis in a 10% SDS polyacrylamide gel followed by semi-dry transfer to a polyvinylidene fluoride membrane. Membranes were blocked in 5% non-fat dry milk in Tris-buffered saline containing 0.2% Tween-20 then incubated with rabbit anti-TH (1:500; Millipore, Burlington, MA), rabbit anti-VMAT2 (1:500, Millipore), or rabbit anti-DAT (1:100, Santa Cruz) overnight followed by incubation in horseradish peroxidase-conjugated secondary antibody (1:5000, Santa Cruz) for one hour. Chemiluminescent detection was performed and analyzed using the ChemiDoc XRX imaging system. Membranes were reprobed with β-actin as a control with all densitometric analysis normalized to β-actin signal using Fiji.

2.13. In vivo immunofluorescence

Free-floating 40 μM coronal sections of SN or ST described above were mounted on positively charged microscope slides and immunolabeled for TH (1:500), MAP2 (1:100, Abcam), 3-nitrotyrosine (3-NT; 1:100, Abcam), GFAP (1:500, Dako), IBA1 (1:100, Wako), TNF (1:100, Cell signaling), and NOS2 (1:100, BD Bioscience) with Alexa Fluor 488, 555, and 647 secondary antibodies (1:500; Invitrogen,). Three serial sections from each brain region per animal were immunolabeled for quantitative studies of glial phenotype. Slides were imaged using a 10× or 40× air plan apochromat objective on a Zeiss Axiovert 200 M inverted fluorescence microscope (Carl Zeiss) for quantitative analysis and BX51 microscope (Olympus) equipped with a Hamamatsu ORCA-Flash4.0 digital CMOS camera, ProScan III stage controller (Prior) and CellSens Dimension software (version 1.12, Olympus) for representative images. All representative images were processed using Fiji with standard background subtraction and contrast enhancement. Montages had further processing of shade correction to account for stitched images. Original hues were altered when indicated to limit the use of red-green combinations and for consistency.

Quantitative analysis of TH intensity in the ST was performed on 10× magnification montages. Randomized images were segmented manually to highlight the ST and an average TH fluorescence intensity generated. Average TH fluorescence intensity was normalized via division by the mean of the average TH intensity of the saline *Ikbk2*$^{F/F}$ processed on the same day to account for inconsistencies in staining or imaging during batch processing.

Generation of total neuronal counts in the SNpc was performed on sections immunolabeled for TH and MAP2. As used for TH cell counts described above, the boundary of the SNpc was determined via 10× magnification montaging and then quantified on random 40× counting frames (100 μM × 100 μM) using Slidebook software. For assessment of gliosis and gliosis expression of TNF and NOS2, slides were imaged using a 40× air plan apochromat objective with analysis determined using Slidebook software. The development of random 40× counting frames (150 μM × 150 μM) was similar to methods used for stereological counting for TH described above. Images were randomized, and images obtained per tissue segmented for the protein of interest. Once segmented, Slidebook generated an object count based on parameters of objects > 300 μM (GFAP) or 200 μM (IBA1). These object counts were summed for a total count per tissue in gliosis analysis and per frame for assessment of TNF and NOS2 intensity. Furthermore, in TNF and NOS2 analysis in GFAP+ cells, the total sum intensity in only GFAP+ cells was calculated and normalized to the total GFAP+ cell count for that image.

2.14. qPCR array analysis

RNA from the SN of *Ikbk2*$^{F/F}$ and *hGfapcre/Ikbk2*$^{F/F}$ mice collected at euthanasia, flash frozen in liquid nitrogen, and stored at −80 °C until homogenized and lysed using a Qiashredder (Qiagen) and then purified using the RNeasy kit (Qiagen). RNA was quantified and converted to cDNA as described above with 250 ng per sample amplified using RT^2 profiler PCR array for NFκB signaling pathway genes (Qiagen PAMM-025z). Gene expression fold change was analyzed using SAbiosciences software with genes divided for biological gene ontology using DAVID Bioinformatics Resources 6.8 (Da Wei Huang and Lempicki, 2009; Huang and Sherman, 2009). Calculation of false discovery rate (FDR) was performed using significance analysis of microarray (SAM) version 5.0 from Stanford University (Tusher et al., 2001).

2.15. Neuronal viability

Primary astrocytes from *Ikbk2*$^{F/F}$ and *hGfapcre/Ikbk2*$^{F/F}$ mice and cortical neurons from wild-type C57/Bl6J mice were cultured in appropriate medium as described in detail above. Neurons were seeded directly onto poly(L-lysine) coated 12-mm glass coverslips at 1 × 10^5 cells/well. At confluency, astrocytes were treated with 10 μM MPTP and 10 pg/ml TNF and 1 ng/ml interferon-gamma (IFNγ) for 8 h; an established protocol known to elicit neuroinflammatory activation in astrocytes (Carbone et al., 2008). Medium was removed, and astrocytes washed 3 times with PBS to prevent carryover of treatment to neurons and then placed in neurobasal media supplemented with 2 mM L-glutamine, B27 supplement, and PSN antibiotic mixture for 24 h. After 24 h, the medium was removed, spun down to remove any cellular debris and placed on cultured neurons for an additional 24 h. After 24 h, neurons were assessed for cellular death via live-cell fluorescence

imaging. Caspase activity was determined using CellEvent caspase-3/7 green detection reagent (Thermofisher) according to manufacturer's instructions, overall cell death with 3 μM propidium iodide (PI; Sigma), and nuclei using 2 μM Hoechst 33342 (Thermofisher). Using a 20× Plan apochromatic air objective, 10–12 fields per treatment were blindly captured and assessed via blind cell counts using Slidebook software. For each genotype and treatment, there was a minimum of 3 biological replicates with 3–4 repetitions of the experiment.

2.16. P65 translocation

Primary astrocytes from *Ikbk2*$^{F/F}$ and *hGfapcre/Ikbk2*$^{F/F}$ mice were seeded directly onto 12 mm glass coverslips at 5×10^4 cells/well and treated with saline or 10 μM MPTP and 10 pg/ml TNF and 1 ng/ml IFNγ for 1 h. Cells were rinsed with PBS and fixed using cold-methanol as described above. Cells were immunolabeled for p65 (polyclonal 1:100, Cell Signaling) and GFAP (monoclonal 1:500, Cell Signaling) with Alexa Fluor 568 and 488 secondary antibodies (Invitrogen), respectively. Using a 40× apochromatic air objective, 10–12 fields per treatment were blindly captured and assessed for positive nuclear p65 per GFAP+ cell per field using Slidebook software. For each genotype and treatment, there was a minimum of 3 biological replicates with 3–4 repetitions of the experiment.

2.17. Inflammatory gene expression in cultured astrocytes

Confluent primary astrocytes cultures from *Ikbk2*$^{F/F}$ and *hGfapcre/Ikbk2*$^{F/F}$ mice were treated with saline or 10 μM MPTP and 10 pg/ml TNF and 1 ng/ml IFNγ for 8 h. Cells were then rinsed with cold PBS and RNA was isolated from glia utilizing the RNeasy Mini Kit (QIAGEN, Valencia, CA) with purity and concentration confirmed using a NanoDrop ND-1000 spectrophotometer. Five hundred ng of RNA was used as a template for reverse transcriptase reactions using the iScript RT kit (Bio-Rad) cDNA was mixed with SYBR Green (Bio-Rad) with primer pairs for *Tnf, Nos2,* interleukin 1-beta (*Il-1β*), interleukin 6 (*Il-6*), chemokine-like ligand 2 and 5 (*Ccl2* and *Ccl5*) as published previously (Kirkley et al., 2017).

2.18. Statistical analyses

All statistical analyses were performed using Prism software (version 6.0; Graphpad Software, Inc., San Diego, CA) with a Student's t-test utilized for comparison of two means, whereas a two-way analysis of variance (ANOVA) followed by a Tukey-Kramer multiple comparison *post-hoc* test was used for comparison of three or more means. Independent variables for two-way ANOVA were defined as genotype (versus *Ikbk2*$^{F/F}$ versus *hGfapcre/Ikbk2*$^{F/F}$) and treatment (saline versus MPTPp). Statistical significance was defined as a p-value < .05 and indicated by asterisks.

3. Results

3.1. Conditional deletion of IKK2 in astrocytes

To study the role of reactive astrogliosis in the onset and progression of PD, we generated a mouse with a conditional deletion of IKK2, an essential kinase involved in the initiation of inflammation in the NFkβ pathway (Bonizzi and Karin, 2004). This was accomplished through breeding *Ikbk2*-floxed mice (Li et al., 2003) with *hGfapcre* transgenic mice expressing Cre under the control of the human *Gfap* promoter (Zhuo et al., 2001; Fig. 1A). Three generations of pairing were required to generate mice that had both the *hGfapcre* allele and were homozygous for floxed-*Ikbk2* (*hGfapcre/Ikbk2*$^{F/F}$) and thus for all experiments littermates homozygous for floxed-Ikbk2, but lacking *hGfapcre*, known as *Ikbk2*$^{F/F}$, were utilized as controls. Genotype assessment for the presence of *hGfapcre* and *Ikbk2*^{F} (Fig. 1B) was achieved through PCR on ear tags in adults and tail biopsies from neonatal mice.

The use of hGfap-Cre mice to target specific deletion in astrocytes has shown conflicting results, with studies reporting non-targeted recombination events in neurons (Zhuo et al., 2001; Malatesta et al., 2003; Casper and McCarthy, 2006). To test the efficiency and specificity of Cre induced recombination in the brain, we cultured primary astrocytes, microglia, and striatal neurons from *Ikbk2*$^{F/F}$ and *hGfapcre/Ikbk2*$^{F/F}$ mice. The purity of cultured astrocytes and microglia was determined using flow cytometry against GLAST for astrocytes and CD11b for possible microglial contamination (Fig. 1C). Both *Ikbk2*$^{F/F}$ and *hGfapcre/Ikbk2*$^{F/F}$ mice had between a 75–78% GLAST positive population and < 10% presence of CD11b + cells. Consistently, *hGfapcre/Ikbk2*$^{F/F}$ astrocyte cultures had less microglia presence than their *Ikbk2*$^{F/F}$ counterparts. Microglia purity was determined to be around 90% (data not shown) for both genotypes.

The deletion of *Ikbk2* at the genomic level in cultured cells was determined utilizing qPCR (Fig. 1D). Cultured astrocytes from *hGfapcre/Ikbk2*$^{F/F}$ neonates showed a deletion rate of 71% for *Ikbk2*^{F} while cultured astrocytes from *hGfapcre/Ikbk2*$^{F/F}$ adults (20 weeks) was slightly reduced to 65% loss of *Ikbk2*^{F}. Cultured microglia and striatal neurons from *hGfapcre/Ikbk2*$^{F/F}$ mice had minimal loss of genomic *Ikbk2* with only 3% and 11% loss, respectively. Astrocytic genomic loss of *Ikbk2* corresponded to a similar loss of IKK2 protein (~70%) measured by western blotting (Fig. 1E & 1F).

We further examined expression of IKK2 via immunofluorescence in primary astrocytes (Fig. 2A & 2B), microglia (Fig. 2C & 2D) and striatal neurons (Fig. 2E & 2F) cultured from *Ikbk2*$^{F/F}$ and *hGfapcre/Ikbk2*$^{F/F}$ neonates and in tissue from the SN (Fig. 2G & 2H) to evaluate mid-brain neurons. Both striatal neurons ($p = 0.88$, N between 5 and 12) and microglia ($p = 0.1204$, N between 9 and 12) from *hGfapcre/Ikbk2*$^{F/F}$ mice showed no significant loss of IKK2 immunolabeling in comparison to cells obtained from *Ikbk2*$^{F/F}$ littermates (Fig. 2I & 2J). This is in sharp contrast to the significant decrease in IKK2 fluorescence seen in astrocytes (Fig. 2l; $p = 0.0023$, N = 6). Furthermore, IKK2 was intact in neurons of the SNpc in adult *hGfapcre/Ikbk2*$^{F/F}$ mice with frequency and intensity of levels of IKK2 not significantly different than *Ikbk2*$^{F/F}$ littermates (Fig. 2J; $p = 0.45$, N between 10 and 12). These data indicate a specific reduction of IKK2 in *hGfapcre/Ikbk2*$^{F/F}$ to astroglial cells within the brain of both neonatal and adult mice.

3.2. Conditional deletion of IKK2 in astrocytes is neuroprotective

After establishing specificity of IKK2 loss in astrocytes, *Ikbk2*$^{F/F}$ and *hGfapcre/Ikbk2*$^{F/F}$ mice were used in an established subacute dosing model of PD whereby the mice were treated over the course of 7 days with probenecid and MPTP (MPTPp) and assessed at the end of dosing (7 days) or a week following cessation of dosing (14 days; Fig. 3A; Miller et al., 2011). To determine the extent of MPTPp induced dopamine neurodegeneration, unbiased, systematic stereological counts of TH+ neurons in the SNpc were performed (Fig. 3). MPTPp-treated Ikbk2$^{F/F}$ mice had a 45% reduction in the number of TH+ cells at day 7 as compared to saline-treated mice (Fig. 3B-D), with a 60% loss in the number of TH+ cells by day 14, even after cessation of MPTPp treatment at day 7. In contrast, *hGfapcre/Ikbk2*$^{F/F}$ mice largely significantly protected from both direct lesioning effects of MPTPp treatment as well as from progressive loss of TH+ neurons from day 7 to day 14, as indicated by preservation of dopaminergic soma in the SNpc (Fig. 3H-J). Quantitative stereological cell counts (Fig. 3T) indicated wild-type *Ikbk2*$^{F/F}$ had a 45% loss of TH+ cells by day 7 and 60% loss by day 14 ($p < 0.0001$, N between 5 and 7), whereas there was no significant loss of TH+ neurons in *hGfapcre/Ikbk2*$^{F/F}$ KO mice at day 7 and significant 36% loss by day 14 ($p = 0.0056$, N between 5 and 7). Analysis by two-way ANOVA revealed an effect of MPTPp treatment on SNpc levels of TH+ neurons ($F(2,25) = 23.29$, $p < 0.0001$) that differed depending on genotype ($F(1,25) = 23.10$, $p < 0.0001$) with the most marked and statistically significant difference observed during the post-lesioning

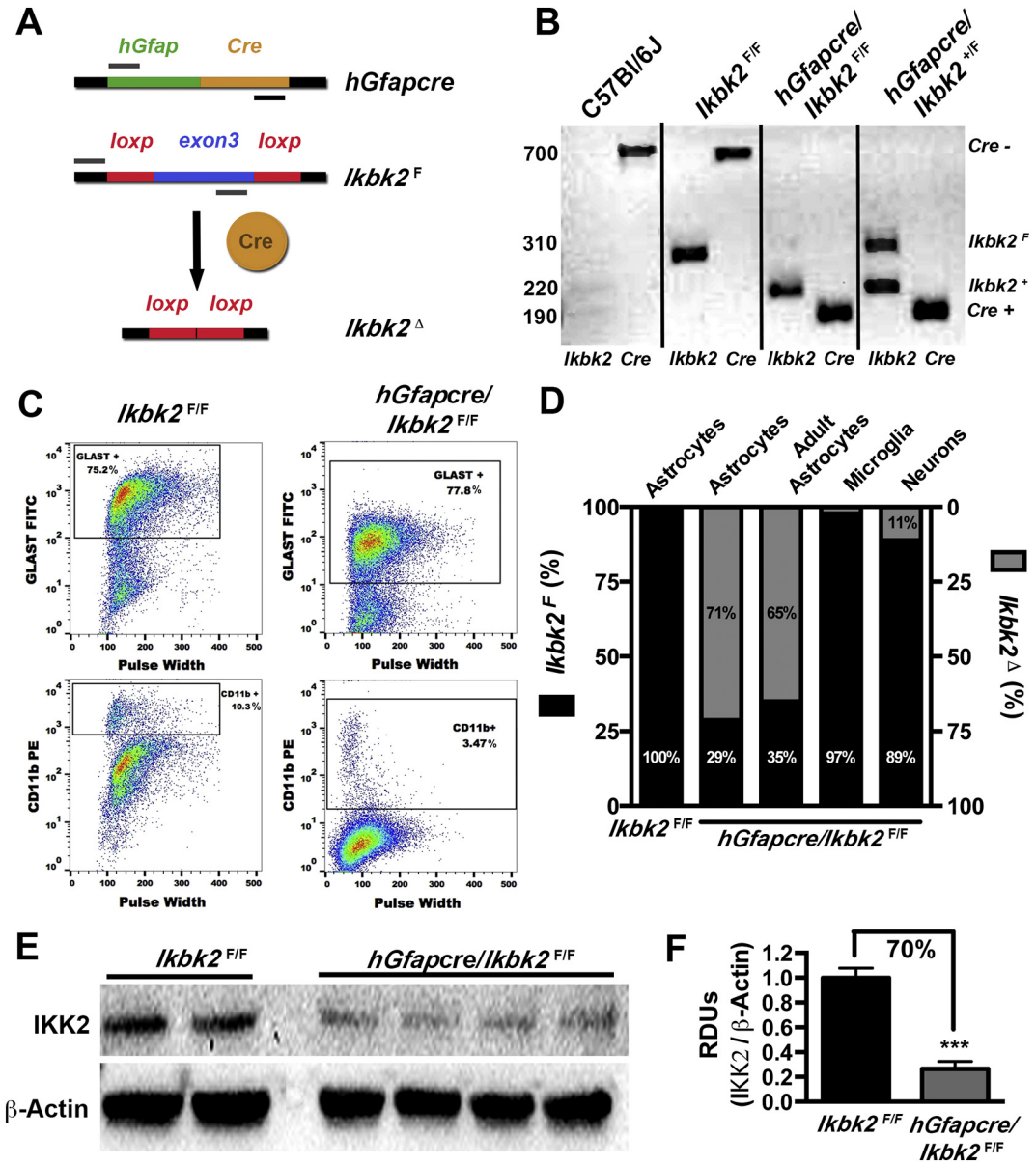

Fig. 1. Astrocyte-specific *Ikbk2* gene deletion in *hGfapcre/Ikbk2*$^{F/F}$ mice. A. Conditional knockout of *Ikbk2* gene in astrocytes was achieved through breeding mice with cyclic recombinase in control of the human glial fibrillary acidic promoter (*hGfapcre*) to mice that were homozygous for a floxed-*Ikbk2* (*Ikbk2*^{F}) gene resulting in deletion of the Ikbk2 (*Ikbk2*$^{\Delta}$). B. *Ikbk2*$^{F/F}$ and *hGfapcre/Ikbk2*$^{F/F}$ mice were genotyped via PCR for the presence of *hGfapcre* allele and presence for floxed (F) or wild-type (+) *Ikbk2* allele. Genotyping of a C57/Bl6/J mouse is provided for reference. C. Primary cultures of astrocytes cultured from *Ikbk2*$^{F/F}$ and *hGfapcre/Ikbk2*$^{F/F}$ mice were assessed for culture purity through flow cytometric analysis for percent GLAST (astrocyte) and CD11b (microglia) expression. D. Genomic DNA from primary astrocytes, microglia, and neurons cultured from neonatal (day 1) and astrocytes cultured from adult (20-week) *Ikbk2*$^{F/F}$ and *hGfapcre/Ikbk2*$^{F/F}$ mice were analyzed via qPCR to assess the rate of *Ikbk2* deletion. Percentages of *Ikbk2*^{F} and *Ikbk2*$^{\Delta}$ are shown in black and grey, respectively. E. Protein isolated from *hGfapcre/Ikbk2*$^{F/F}$ *and Ikbk2*$^{F/F}$ cultured astrocytes was analyzed for the amount of IKK2 via western blot. **F.** IKK2 protein levels were quantified using densitometric analysis with normalization to levels of β-Actin. Data are presented as mean ± SEM with *Ikbk2*$^{F/F}$ (black bars) and *hGfapcre/Ikbk2*$^{F/F}$ (grey bars; Student *t*-test. *** $p < 0.001$).

progression phase at days 7–14 in wildtype mice.

In addition to TH+ cell counts, total neuronal counts via MAP2 immunofluorescence of the SNpc and TH intensity of the ST were assessed (Fig. 3). Following similar trends to TH counts, MPTPp-treated *Ikbk2*$^{F/F}$ mice had marked reductions in the number of MAP2+ cells at day 7 with the number of TH+ cells continuing to decline from day 7–14 (Fig. 3E-G; $p = .024$, N between 5 and 7) while MPTP-treated *hGfapcre/Ikbk2*$^{F/F}$ mice had a more minimal, yet significant loss of MAP2+ cells (Fig. 3K-M; $p = 0.03$, N between 5 and 7). Analysis via a two-way ANOVA revealed a substantial effect on MPTPp treatment ($F(2,24) = 13.24$, $p = 0.0001$) and genotype ($F(1,24) = 9.06$, $p = 0.0061$) of MAP2 levels in the SNpc (Fig. 3U). Loss of TH intensity in the ST after MPTPp treatment also revealed marked loss in MPTPp-treated *Ikbk2*$^{F/F}$ mice (Fig. 3N-P; $p = 0.027$, N = 6) that was greatly diminished in *hGfapcre/Ikbk2*$^{F/F}$ mice (Fig. 3Q-S). Analysis of fluorescence intensity of striatal TH by two-way ANOVA indicated a significant loss of striatal TH in the post-lesioning phase in *Ikbk2*$^{F/F}$ mice, but not in *hGfapcre/Ikbk2*$^{F/F}$ mice (Fig. 3V; $p = 0.033$, N = 6).

3.3. Conditional deletion of IKK2 in astrocytes protects against MPTPp induced changes in locomotor function and striatal protein loss but not Striatal Catecholamines

MPTP treatment in rodents is known to severely damage

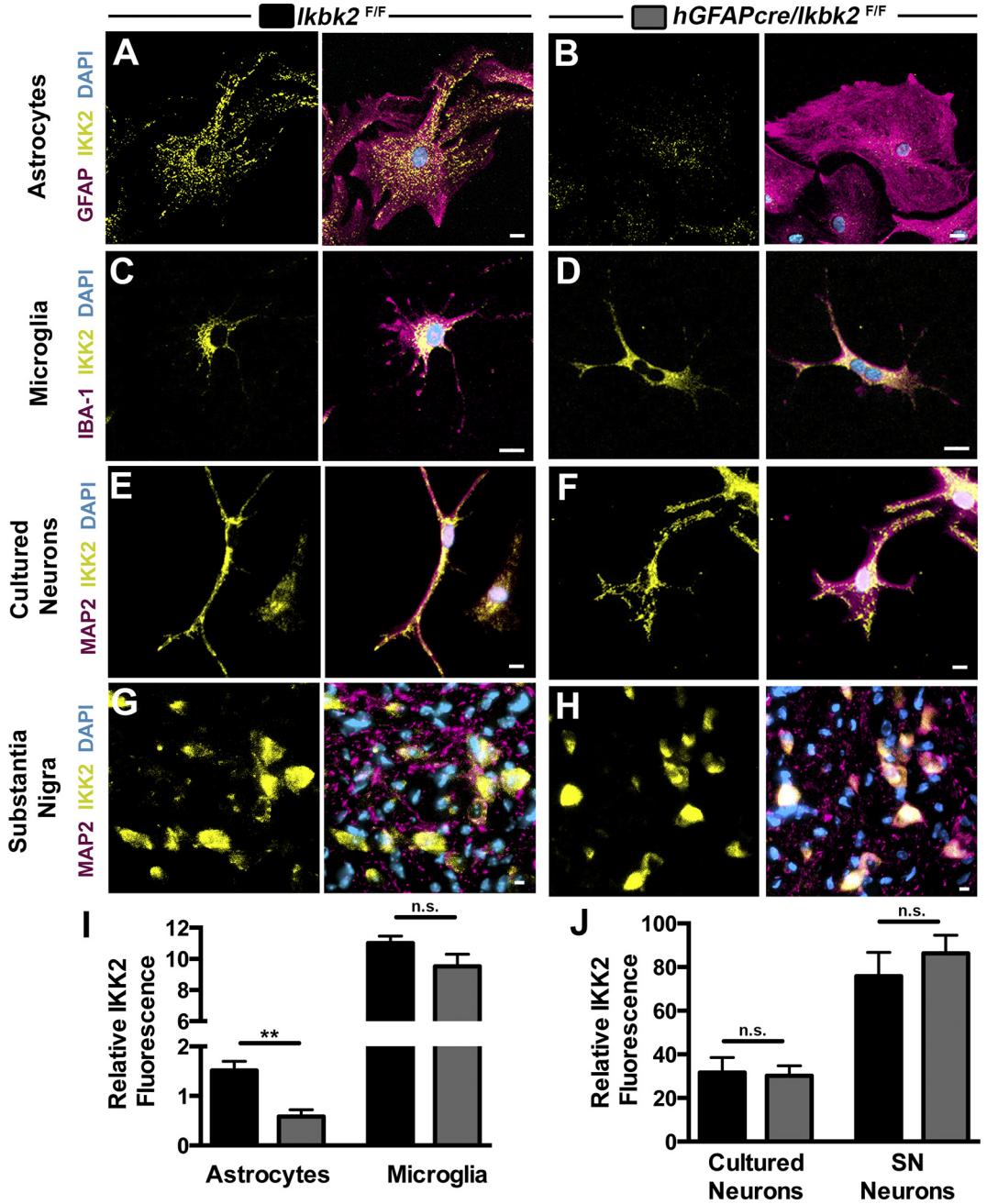

Fig. 2. Astrocyte-specific deletion of IKK2 in *hGfapcre/Ikbk2*$^{F/F}$ mice. Cell-specific IKK2 expression in astrocytes, microglia, and neurons cultured from *Ikbk2*$^{F/F}$ (A, C, E) and *hGfapcre/Ikbk2*$^{F/F}$ (B, D, F) mice were immunolabeled for IKK2 (yellow), cell-specific markers (magenta) for astrocytes (GFAP; A and B), microglia (IBA1; C and D), or neurons (MAP2, E and F) and counterstained with DAPI (cyan) to visualize cell nuclei. Scale bar = 10 μm. G-H. Representative 40× images of colocalization of MAP2+ neurons (magenta) and IKK2 (yellow) in the substantia nigra (SN) of adult *Ikbk2*$^{F/F}$ (G) and *hGFAP-Cre/Ikbk2*$^{F/F}$(H) mice. Cyan = DAPI. Q - R. The mean IKK2 fluorescence intensity (with background subtraction) between *Ikbk2*$^{F/F}$(black bars) and *hGfapcre/Ikbk2*$^{F/F}$(grey bars) was measured in astrocytes and microglia (Q) and in cultured neurons versus SN neurons (R). Data are presented as mean fluorescence intensity ± SEM. (Student *t*-test; ** $p < 0.01$ and n.s. = not significant). (For interpretation of the references to colour in this figure legend, the reader is referred to the web version of this article.)

dopaminergic terminals in the striatum producing losses in catecholamines and DA-associated proteins that are linked to acute changes in locomotor behavior (Fredriksson et al., 1990). Striatal levels of DA and its metabolites, DOPAC and HVA, were measured in *Ikbk2*$^{F/F}$ and *hGfapcre/Ikbk2*$^{F/F}$ mice via HPLC following lesioning with MPTPp (Fig. 4A-D). Levels of DA were significantly decreased at day 7 in *Ikbk2*$^{F/F}$ ($p = 0.027$, N = 5) and *hGfapcre/Ikbk2*$^{F/F}$ mice ($p < 0.0001$, N = 5), with continued, but no further reduction, at day 14 (Fig. 4A; $p < 0.017$ and $p < 0.0001$, respectively). There were no significant differences in DA loss between genotypes; however, MPTPp-treated *hGfapcre/Ikbk2*$^{F/F}$ mice trended toward higher recovery at 14 days than their wild-type *Ikbk2*$^{F/F}$ littermate genotype controls. Similar patterns were observed for the dopamine metabolites DOPAC (Fig. 4B) and HVA (Fig. 4D). Measurements of the DOPAC to DA ratio were unchanged by treatment and were not different between genotypes (Fig. 4C).

The effects of MPTPp on neurobehavioral function in *Ikbk2*$^{F/F}$ versus *hGfapcre/Ikbk2*$^{F/F}$ mice were determined by open-field activity measurements and video recordings of stride length (Fig. 4E-H). In comparison to baseline measurements recorded at day 0, only *Ikbk2*$^{F/F}$ mice exposed to MPTPp had significant depression of spontaneous locomotor

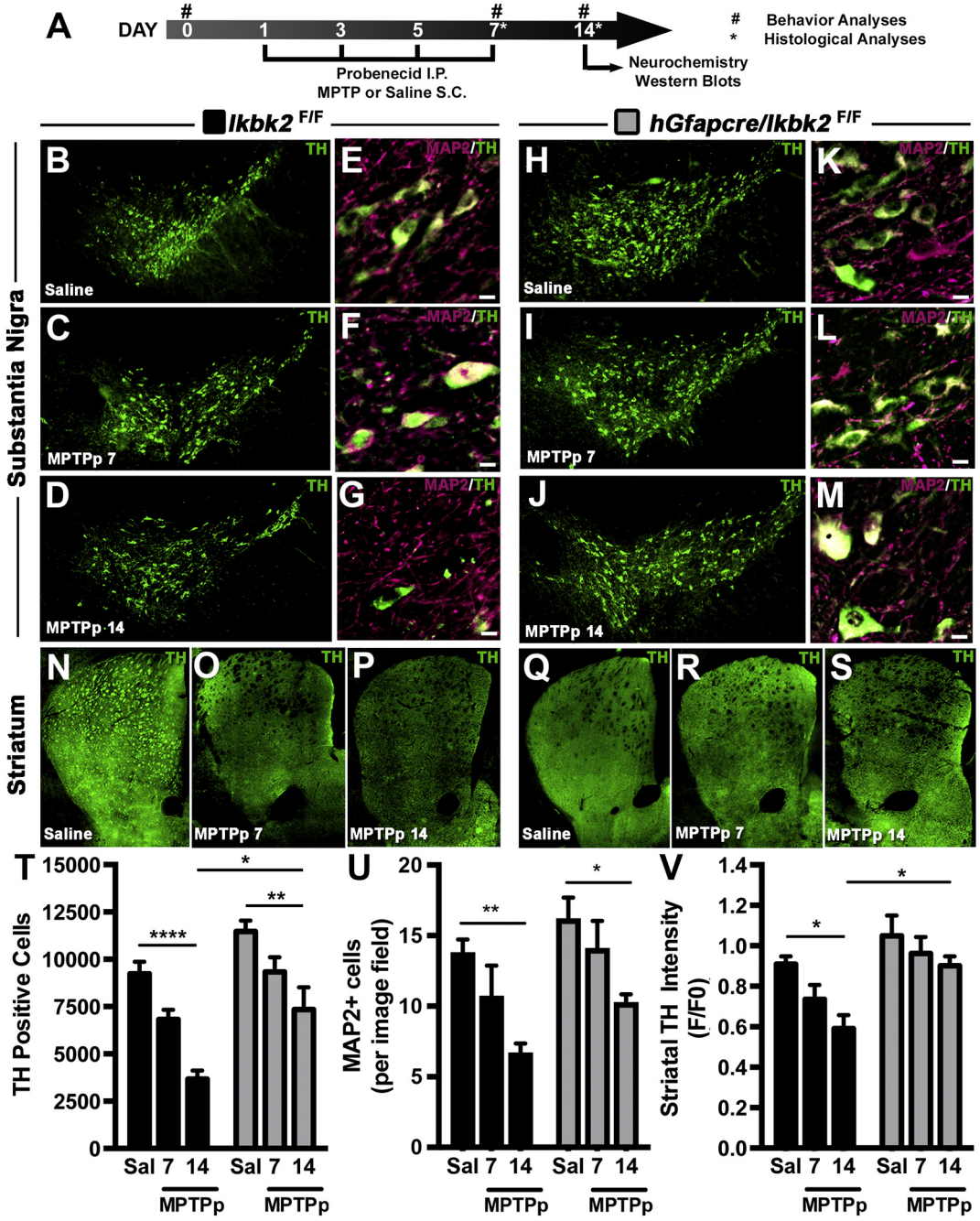

Fig. 3. MPTP-induced loss of dopaminergic neurons and neuronal projections is decreased in *hGfapcre/Ikbk2*$^{F/F}$ mice. A. Schematic of treatment and experimental regimen for the study. B-M. The number of TH+ neurons (green) in the substantia nigra pars compacta (SNpc) was assessed via immunofluorescence-based stereology and presented as representative montages for *Ikbk2*$^{F/F}$ (B-D) and *hGFAP-Cre/Ikkβ*$^{F/F}$ mice (H-J). Total neuronal loss was determined via counts of MAP2+ neurons within the SNpc through immunofluorescence and presented as representative images showing MAP2 (magenta) and TH (green) for *Ikbk2*$^{F/F}$ (*E*-G) and *hGFAP-Cre/Ikkβ*$^{F/F}$ mice (K-M). N-S. Loss of dopaminergic nerve terminals was assessed via quantification of immunofluorescence intensity of TH in the striatum (ST) as shown in representative montages for *Ikbk2*$^{F/F}$ (N–P) and *hGFAP-Cre/Ikkβ*$^{F/F}$ mice (Q-S). T. Quantitative stereological counts estimating the total number of TH+ neurons presented as an average number of TH+ cells ± SEM. U. Quantitative counts of MAP2+ neurons to estimate total neuronal loss presented as an average number of MAP2+ cells per image field ± SEM. V. Loss of striatal TH intensity was quantified via measuring total striatal TH intensity and normalized to saline *Ikbk2*$^{F/F}$ mice. Data is presented as average TH intensity ± SEM. Data was analyzed by two-way ANOVA with Tukey-Kramer post hoc test (* $p < 0.05$, ** $p < 0.01$, and **** $p < 0.0001$). (For interpretation of the references to colour in this figure legend, the reader is referred to the web version of this article.)

activity observed at day 7 (N between 10 and 21) compared with their saline controls, whereas MPTPp-treated *hGfapcre/Ikbk2*$^{F/F}$ mice displayed no changes in locomotion. Analysis via two-way ANOVA showed significant effects with treatment for total distance traveled (Fig. 4E; F(1.57) = 4.63, $p = 0.036$), rearing number (Fig. 4G; F(1.57) = 12.13, $p = 0.001$), and stride length (Fig. 4H; F(1.57) = 9.31, $p = 0.004$) but not for movement time (Fig. 4F; F(1.57) = 0.84, $p = 0.36$) and margin time (data not shown). Changes in these parameters over time are depicted in Fig. 4I–L. Genotype had a significant effect with total distance traveled (F(1.57) = 12.30, $p = 0.0009$), movement time (F(1.57) = 12.89, $p = 0.0007$), margin time (F(1.57) = 7.31, $p = 0.009$) and stride length (F(1.57) = 6.47, $p = 0.014$), but not in rearing number (F(1.57) = 3.35, $p = 0.07$). Only total distance traveled showed an interaction between treatment and genotype (F

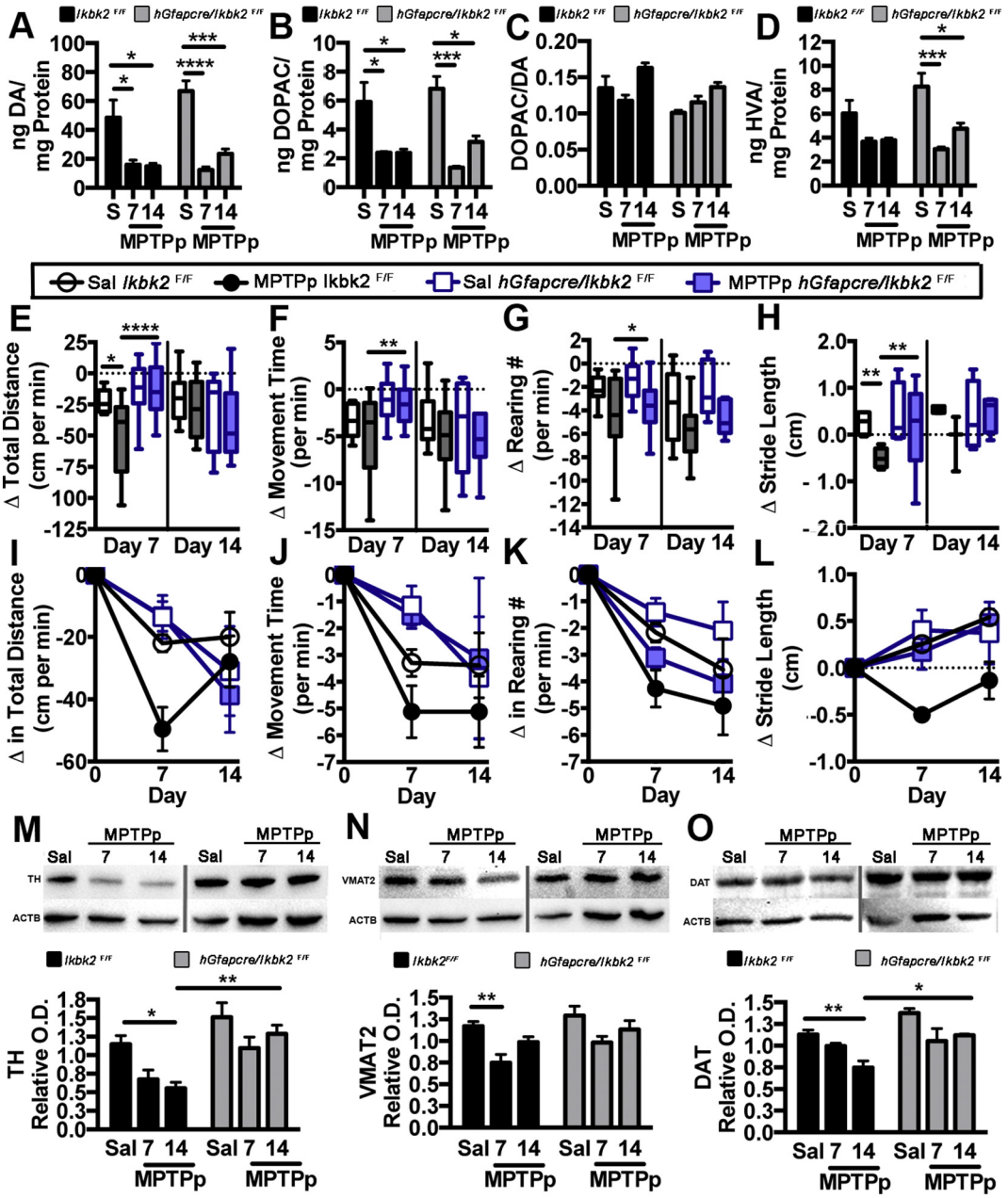

Fig. 4. *hGfapcre/Ikbk2*$^{F/F}$ mice are protected from MPTP-induced locomotor changes and striatal protein losses but not from loss of striatal dopamine (DA) and its metabolites. A-D. Striatal levels of DA (A), its metabolites DOPAC (B) and HVA (D) were analyzed via HPLC. The rate of dopamine metabolism was determined by measuring the DOPAC/DA (C). Data are presented as mean ± SEM. E-L. Changes in open field locomotion and stride length were monitored in *Ikbk2*$^{F/F}$ and *hGfapcre/Ikbk2*$^{F/F}$ mice at days 0, 7, and 14. Changes in total distance moved (E, I), time spent moving (F, J), number of rearing movements (G, K) and stride length (H, L) are expressed between groups (E-H) and over time (I-L) and represented as the average change from baseline (day 0) ± SEM. M-O. Levels of TH (M), VMAT2 (N), and DAT (O) from the striatum of *Ikbk2*$^{F/F}$ (black bars) and *hGfapcre/Ikbk2*$^{F/F}$ mice (grey bars) were assessed via western blot and quantified using densitometric analysis with normalization to levels of β-Actin (ACTB). Data was analyzed by two-way ANOVA with Tukey-Kramer post hoc test (* $p < 0.05$, ** $p < 0.01$, *** $p < 0.001$ and **** $p < 0.0001$).

(1.57) = 4.63, $p = 0.033$). *Post-hoc* analysis revealed that decreases in all neurobehavioral parameters analyzed in MPTPp-treated *Ikbk2*$^{F/F}$ mice were statistically different from MPTPp-treated *hGfapcre/Ikbk2*$^{F/F}$ mice at day 7 ($p < 0.05$). However, there was not a significant effect on these parameters by day 14 for treatment or genotype with *post-hoc* analysis revealing no differences in the behavioral scores of *Ikbk2*$^{F/F}$ and *hGfapcre/Ikbk2*$^{F/F}$ mice.

Levels of DA associated striatal proteins were determined through western blotting of flash-frozen striatal tissue from *Ikbk2*$^{F/F}$ and *hGfapcre/Ikbk2*$^{F/F}$ mice collected at day 7 and day 14 post-treatment (Fig. 4M-O). Wild type *Ikbk2*$^{F/F}$ mice treated with MPTPp showed significant reduction in protein levels of TH (Fig. 4M; day 14 $p = 0.025$, N = 7), VMAT2 (Fig. 4N; day 7 $p = 0.0094$, N = 7), and DAT (Fig. 4O; day 14 $p = 0.0071$, N = 7) compared to saline controls whereas *hGfapcre/Ikbk2*$^{F/F}$ mice treated with MPTPp had no significant loss. Analysis of densitometry via two-way ANOVA indicated that treatment (TH F(2, 33) = 7.0, $p = 0.0029$; VMAT F(2,33) = 9.56, $p = 0.0005$); and DAT F(2,33) = 69.87, $p = .0004$) and genotype (TH F(1, 33) = 22.07, $p < 0.0001$; VMAT F(1,33) = 5.85, $p = 0.021$; and DAT F(1,33) = 14.10, $p = 0.0007$) had significant effects on all proteins with *post-hoc* analysis revealing significant differences in TH ($p = 0.005$) and DAT ($p = 0.013$) in day 14 of MPTPp-treated *Ikbk2*$^{F/F}$

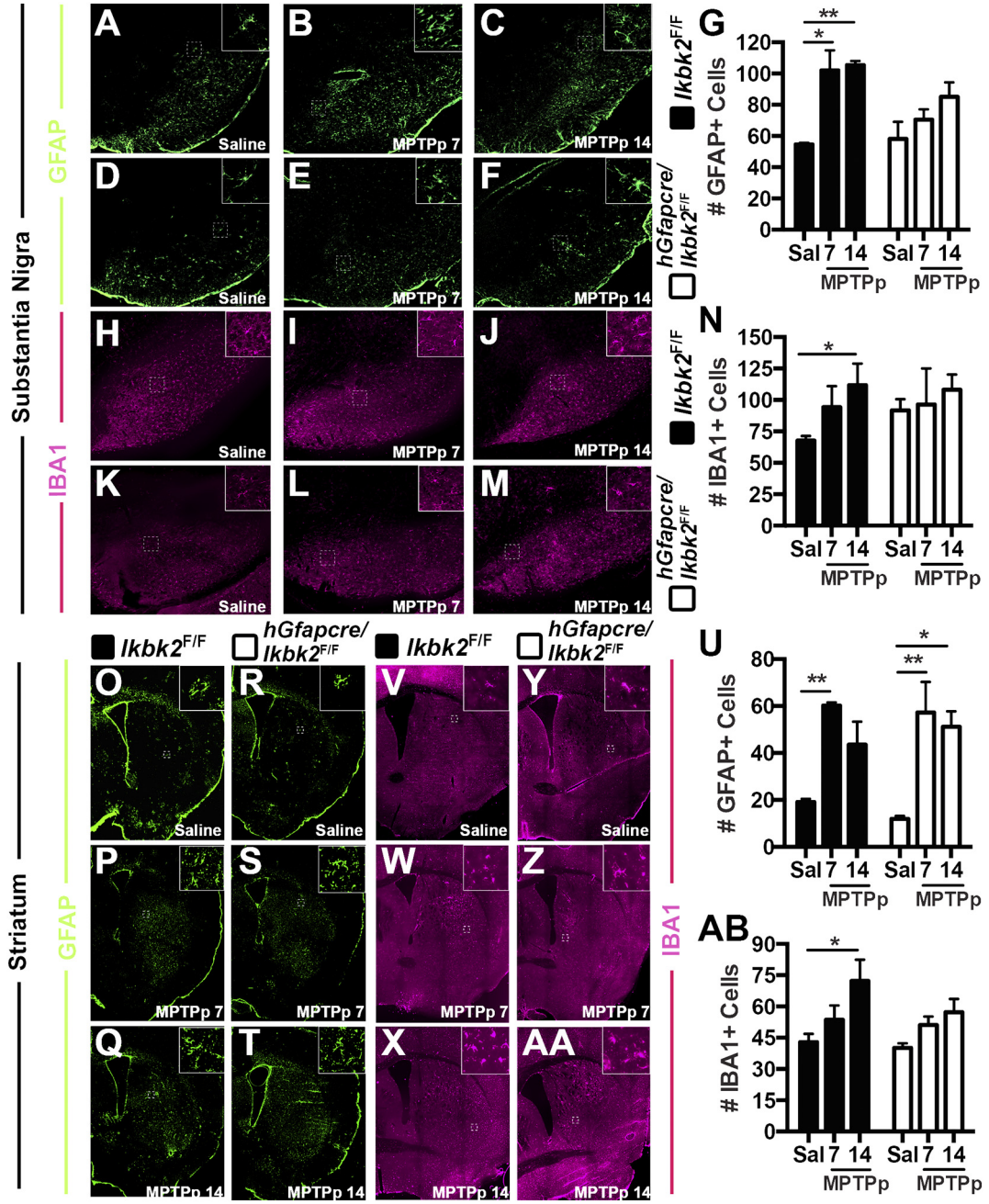

Fig. 5. MPTP-induced gliosis is partially reduced in *hGfapcre/Ikbk2*$^{F/F}$ mice. Gliosis following saline or MPTPp treatment was quantified via counts of positively immunolabeled cells for GFAP (astrocytes) and IBA1 (microglia) in the SN and ST of *Ikbk2*$^{F/F}$ (black bars) and *hGfapcre/Ikbk2*$^{F/F}$ (grey bars). A-F. Representative montages of GFAP + cells (green) in the SN of *Ikbk2*$^{F/F}$ (A-C) and *hGfapcre/Ikbk2*$^{F/F}$ (D-F) mice. G. Quantitative counts of GFAP + cells in the SN presented as mean counts ± SEM. H-M. Representative montages of IBA1 + cells (magenta) in the SN of *Ikbk2*$^{F/F}$ (H-J) and *hGfapcre/Ikbk2*$^{F/F}$ (K-M) mice. N. Quantitative counts of IBA1 + cells in the SN presented as mean counts ± SEM. O-T. Representative montages of GFAP + cells (green) in the ST of *Ikbk2*$^{F/F}$ (O-Q) and *hGfapcre/Ikbk2*$^{F/F}$ (R-T) mice. U. Quantitative counts of GFAP + cells in the ST presented as mean counts ± SEM. V-AA. Representative montages of IBA1 + cells (magenta) in the ST of *Ikbk2*$^{F/F}$ (V-X) and *hGfapcre/Ikbk2*$^{F/F}$ (Y-AA) mice. AB. Quantitative counts of IBA1 + cells in the ST presented as mean counts ± SEM. Data was analyzed by two-way ANOVA with Tukey-Kramer post hoc test (* $p < 0.05$, ** $p < 0.01$ and ***$p < 0.001$). (For interpretation of the references to colour in this figure legend, the reader is referred to the web version of this article.)

and *hGfapcre/Ikbk2*$^{F/F}$ mice.

3.4. Conditional deletion of IKK2 in astrocytes results in attentuated glial activation in the substantia nigra and striatum after treatment with MPTP

To assess glial activation in response to neuronal injury, cryo-preserved frozen serial sections of SN and ST from *Ikbk2*$^{F/F}$ and *hGfapcre/Ikbk2*$^{F/F}$ mice treated in the MPTPp dosing model were assessed for the number of astrocytes and microglia utilizing immunolabeling for GFAP and IBA1, respectively (Fig. 5, N between 5 and 8). Within the SN of *Ikbk2*$^{F/F}$ mice, representative montages for GFAP reveal a visible increase in the number of GFAP + cells in response to MPTPp treatment as compared to saline (Fig. 5A), that was maximal by day 7 (Fig. 5B) and did not further increase by day 14 (Fig. 5C). The SN of *hGfapcre/Ikbk2*$^{F/F}$ mice showed similar basal levels of GFAP + cells in saline-treated mice (Fig. 5D) that showed a trend toward increase following MPTPp treatment from day 7 (Fig. 5E) to day 14 (Fig. 5F), although this increase was not statistically significant, in contrast to their wild-type

littermate counterparts. Analysis of quantitative GFAP+ counts by two-way ANOVA (Fig. 5G) indicate both a statistical effect of treatment ($F(2, 26) = 8.94$, $p = 0.0011$) and genotype ($F(1, 26) = 4.23$, $p = 0.05$), with *post-hoc* analysis revealing increases in numbers of GFAP+ cells from saline in day 7 ($p = 0.012$) and day 14 ($p = 0.006$) MPTPp treated *Ikbk2*$^{F/F}$ mice. These data indicate that deletion of astrocyte IKK2 is protective against astrocytic activation and that MPTPp did not cause any further increase in GFAP+ cells within a week of treatment in *Ikbk2*$^{F/F}$ mice.

The microglial response in the SN was determined by counting cells positively immunolabeled for IBA1 (Fig. 5H-N; N between 5 and 8). Within the SN of *Ikbk2*$^{F/F}$ mice, representative montages for IBA1 reveal a visible increase in the number of IBA1+ cells in response to MPTPp treatment as compared to saline (Fig. 5H) with progressive increases in IBA1 immunolabeling from day 7 (Fig. 5I) to day 14 (Fig. 5J). In contrast, the SN of *hGfapcre/Ikbk2*$^{F/F}$ mice showed slightly higher basal levels of IBA1+ cells in saline-treated mice (Fig. 5K) that did not change with MPTPp treatment at either day 7 (Fig. 5L) or day 14 (Fig. 5M). Analysis of quantitative IBA1+ counts by two-way ANOVA with *post-hoc* analysis (Fig. 5N) revealing the only significant increases in IBA1 from saline occurred in MPTPp-treated *Ikbk2*$^{F/F}$ mice at day 14 ($p = 0.047$). These data indicate that deletion of IKK2 in astrocytes prevents microglial activation upon MPTPp treatment and may also have a role in limiting microglial numbers in basal conditions.

Astrogliosis was also assessed within the ST of *Ikbk2*$^{F/F}$ and *hGfapcre/Ikbk2*$^{F/F}$ mice (Fig. 5O-AB, N between 5 and 6). Within the ST of *Ikbk2*$^{F/F}$ mice, representative montages for GFAP reveal a visible increase in the number of GFAP+ cells in response to MPTPp treatment as compared to saline (Fig. 5O), with loss of GFAP immunolabeling from day 7 (Fig. 5P) to day 14 (Fig. 5Q). The ST of *hGfapcre/Ikbk2*$^{F/F}$ mice showed similar basal levels of GFAP+ cells in saline-treated mice (Fig. 5R) that were expanded upon MPTPp treatment with no progression from day 7 (Fig. 5S) to day 14 (Fig. 5T) and at similar levels as their *Ikbk2*$^{F/F}$ genotype control counterparts. Analysis of quantitative GFAP+ counts by two-way ANOVA (Fig. 5U) indicate a statistical effect of only treatment ($F(2,25) = 17.75$, $p < 0.0001$) with *post-hoc* analysis revealing significant increases in GFAP numbers from saline in MPTPp treated *Ikbk2*$^{F/F}$ mice at day 7 ($p = 0.0092$) and at both day 7 ($p = 0.0036$) and day 14 ($p = 0.014$) of MPTPp-treated *hGfapcre/Ikbk2*$^{F/F}$ mice. These data indicate that deletion of astrocyte IKK2 is not protective against astrogliosis in the ST in response to MPTPp treatment.

The microglial response in the ST was also determined through counts of positively immunolabeled IBA1 cells (Fig. 5V-AB, N = 6). Within the ST of *Ikbk2*$^{F/F}$ mice, representative montages for IBA1 reveal a visible increase in the number of IBA1+ cells in response to MPTPp treatment as compared to saline (Fig. 5V) with progressive increases in IBA1 immunolabeling from day 7 (Fig. 5W) to day 14 (Fig. 5X). In the ST of *hGfapcre/Ikbk2*$^{F/F}$ mice, basal levels of IBA1+ cells in saline-treated mice (Fig. 5Y) were similar to their wild-type counterparts that increased minimally with MPTPp treatment at either day 7 (Fig. 5Z) to day 14 (Fig. 5AA). Analysis of quantitative IBA1+ counts by two-way ANOVA (Fig. 5AB) indicate a statistical effect of treatment ($F(2,30) = 7.109$, $p = 0.003$) with *post-hoc* analysis revealing significant increases in IBA1+ cells from saline in MPTPp treated *Ikbk2*$^{F/F}$ mice at day 14 ($p = 0.023$). These data indicate that deletion of astrocyte IKK2 is protective against microgliosis in the ST upon MPTPp treatment.

Glial activation itself does not necessarily indicate neuroinflammatory damage, because different states of glial activation can alter the dynamics of tissue repair and response to damage (Burda and Sofroniew, 2014). Thus, to determine if MPTPp-induced expression of inflammatory genes in astrocytes was suppressed with deletion of IKK2, we examined astrocyte-specific expression of NOS2/iNOS (Supplemental Fig. 1; $N = 4$) and TNF (Supplemental Fig. 2; $N = 4$) using co-immunofluorescence in the SN and ST of *Ikbk2*$^{F/F}$ and *hGfapcre/Ikbk2*$^{F/F}$. Levels of NOS2 in GFAP+ cells of the SN of *Ikbk2*$^{F/F}$ mice were minimal in saline-treated mice (Supp. Fig. 1A) but highly increased upon exposure to MPTPp with progressive increases from day 7 (Supp. Fig. 1B) to day 14 (Supp. Fig. 1C). In contrast, NOS2 levels in GFAP+ cells of the SN of *hGfapcre/Ikbk2*$^{F/F}$ mice were not detectable in either saline (Supp. Fig. 1D) or in day 7 (Supp. Fig. 1E) or day 14 (Supp. Fig. 1F) of MPTPp-treated mice. Similar trends were seen in the ST of *Ikbk2*$^{F/F}$ (Supp. Fig. 1G-I) and *hGfapcre/Ikbk2*$^{F/F}$ (Supp. Fig. 1J-L) mice. Levels of TNF in GFAP+ cells of the SN of *Ikbk2*$^{F/F}$ mice were minimal in saline-treated mice (Supp. Fig. 2A) and at day 7 in MPTPp-treated mice (Supp. Fig. 2B) but were greatly increased by day 14 after MPTPp treatment (Supp. Fig. 2C). In contrast, expression of TNF in the SN in GFAP+ cells of *hGfapcre/Ikbk2*$^{F/F}$ mice was not detectable in either the saline group (Supp. Fig. 2D) or at day 7 (Supp. Fig. 2E) or day 14 (Supp. Fig. 2F) in MPTPp-treated mice. Similar trends were seen in the ST of *Ikbk2*$^{F/F}$ mice (Supp. Fig. 2G-I) and *hGfapcre/Ikbk2*$^{F/F}$ mice (Supp. Fig. 2J-L) but with expression of TNF only trending upward in MPTPp-treated *Ikbk2*$^{F/F}$ mice. Quantitative analysis of NOS2 and TNF immunofluorescence indicated that the large increases in expression of NOS2 and TNF in WT mice by day 14 were completely inhibited in *hGfapcre/Ikbk2*$^{F/F}$ mice (Supp. Fig. 1 Mn; Supp. Fig. 2M,N).

3.5. Conditional deletion of IKK2 in astrocytes reverses MPTPp-induced changes in NFκB gene expression

NFκB is involved in regulating numerous biological pathways, including apoptosis and inflammation, which are important pathological mechanisms underlying neurodegeneration in PD (Mattson and Camandola, 2001). To assess transcriptional changes in NFκB-regulated genes involved in apoptosis and inflammation at day 14 following MPTPp treatment, RNA in SN tissue from *Ikbk2*$^{F/F}$ and *hGfapcre/Ikbk2*$^{F/F}$ mice was purified and assessed by qPCR microarray analysis (Fig. 6; N = 4). Heat map analysis of apoptotic genes expressed in the NFκB signaling pathway (Fig. 6A) revealed 1st order clustering of saline-treated *Ikbk2*$^{F/F}$ and MPTPp-treated *hGfapcre/Ikbk2*$^{F/F}$ mice and 2nd order clustering with saline-treated *hGfapcre/Ikbk2*$^{F/F}$ mice with MPTPp-treated *Ikbk2*$^{F/F}$ mice clustering outside all groups. Heat map analysis of inflammatory gene expression regulated by NFκB (Fig. 6B) revealed 1st order clustering of saline-treated *hGfapcre/Ikbk2*$^{F/F}$ and MPTPp-treated *hGfapcre/Ikbk2*$^{F/F}$ mice and 2nd order clustering with saline-treated *Ikbk2*$^{F/F}$ mice with MPTPp-treated *Ikbk2*$^{F/F}$ mice clustering outside all groups. This indicates that in both gene arrays, MPTP-treated *Ikk2* knockout mice clustered with the control group. Interestingly, MPTPp-treated *Ikbk2*$^{F/F}$ and MPTPp-treated *hGfapcre/Ikbk2*$^{F/F}$ mice clustered on opposing ends of the apoptotic and inflammatory heat maps with almost reversed fold-regulation of assessed genes, indicating that IKK2 knockout mice treated with MPTPp had patterns of gene expression more similar to saline-treated controls. Analysis of fold-expression changes in genes expressed in the NFκB signaling pathway were deemed significant if *p*-values were < 0.05 and had a > 1.5-fold change in expression as represented by colored red (up) or blue (down) in volcano plots in Fig. 6D-6G, with genes with an FDR < 0.05 are indicated with an asterisk (*). Fold-regulation of all genes with *p*-values < .05 are shown in bar graphs. In wild-type *Ikbk2*$^{F/F}$ mice, treatment with MPTPp resulted in upregulation of 4 genes NFκB inhibitor alpha (*Nfkbia), IKK1/IKKalpha(Chuk),IKKgamma (Ikbkg) and BCL-2 related protein A1 (Bcl2a1a)* and down-regulation of 3 genes including the caspase recruitment domain-containing protein 1 (*Card11*), epidermal growth factor receptor *(Egfr)* and transcription factor Relb (*Relb)*. Control *hGfapcre/Ikbk2*$^{F/F}$ mice only had significant down-regulation of 2 genes compared to saline *Ikbk2*$^{F/F}$ mice, *Ikbk2* and interferon regulatory factor (*Irf1*) (Fig. 6E). With MPTPp treatment, *hGfapcre/Ikbk2*$^{F/F}$ mice had 2 genes upregulated, TNF superfamily member 10 (*Tnfsf10)* and *Bcl2a1a* and down-regulation of 1 gene, *Egfr,* as compared to saline *Ikbk2*$^{F/F}$ mice (Fig. 6F). Interestingly, comparison of gene expression patterns between MPTPp-treated *Ikbk2*$^{F/F}$ and *hGfapcre/Ikbk2*$^{F/F}$ mice revealed upregulation of only 1 gene, TNF receptor association factor 5

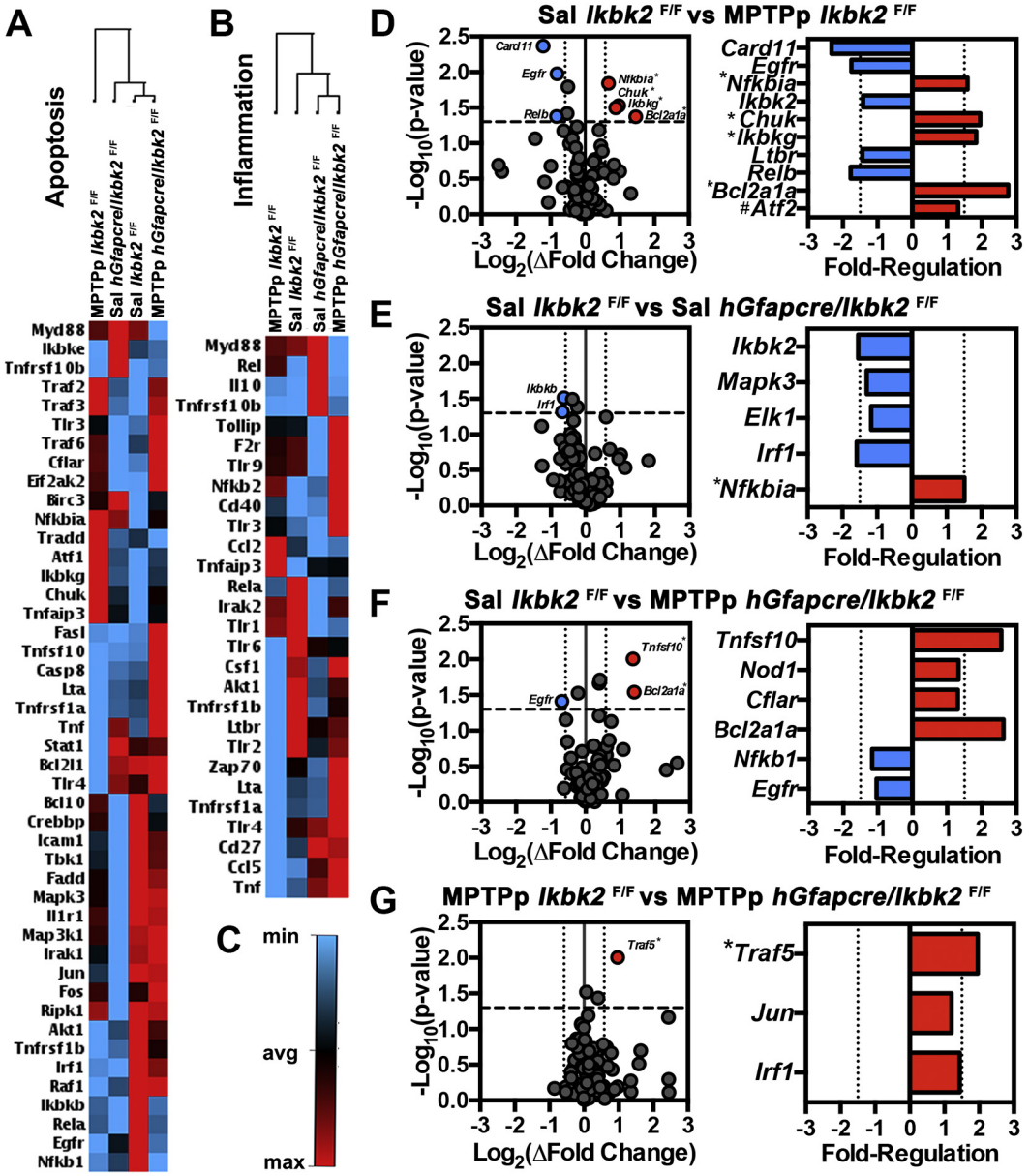

Fig. 6. Microarray analysis of NFκB signaling pathway genes from the SN following MPTPp treatment. Following saline or MPTPp treatment, mRNA from SN's from *Ikbk2*$^{F/F}$ and *hGfapcre/Ikbk2*$^{F/F}$ mice were analyzed in an NFκB signaling microarray for alterations in inflammatory and apoptotic genes. A. Heat map representing fold regulation changes in NFκB signaling genes involved in apoptosis B. Heat map representing fold regulation changes in NFκB signaling genes involved in inflammation C. Colour guide to heat maps with blue representing down-regulation and red indicating up-regulation D-E. Volcano plots (right) and fold regulation graphs (left) for changes in NFκB signaling genes for MPTPp treated *Ikbk2*$^{F/F}$ mice (D), saline-treated *hGfapcre/Ikbk2*$^{F/F}$ mice (E), and MPTPp treated *hGfapcre/Ikbk2*$^{F/F}$ mice (F) in comparison to saline-treated *Ikbk2*$^{F/F}$ mice. G. Volcano plots (right) and fold regulation graphics (left) for changes in NFκB signaling genes in MPTPp treated *hGfapcre/Ikbk2*$^{F/F}$ mice in comparison to MPTPp treated *Ikbk2*$^{F/F}$ mice. Volcano plots represent all genes evaluated in the microarray with colored dots meeting criteria of a p-value < .05 on (y-axis) and fold change above 1.5 (x-axis) while fold regulation is only genes whose p-value was < 0.05. All data was analyzed using SA biosciences software. * indicates that the calculated FDR was also < 0.05. # indicates a FDR < 0.05 but a *p* above 0.05. (For interpretation of the references to colour in this figure legend, the reader is referred to the web version of this article.)

(*Traf5*) in *hGfapcre/Ikbk2*$^{F/F}$ mice as compared to *Ikbk2*$^{F/F}$ mice (Fig. 6G).

3.6. Neurons are protected against MPTPp induced 3-NT and Caspase Activation with Loss of Astrocytic IKK2

Given that deletion of IKK2 in astrocytes suppressed both glial activation and changes in expression of genes regulating inflammation and neuronal apoptosis in vivo, we wanted to determine whether attenuation of innate immune responses in astrocytes would directly modulate neuronal viability during treatment with MPTPp both in vivo and in vitro. The number of TH+ neurons containing 3-nitrotyrosine as a measure of oxidative/nitrosative stress in the SNpc was measured by co-immunofluorescence in *Ikbk2*$^{F/F}$ and *hGfapcre/Ikbk2*$^{F/F}$ mice following exposure to MPTPp (Fig. 7A-E; N between 4 and 7). As shown in representative 40× images, MPTPp treatment in *Ikbk2*$^{F/F}$ mice drastically elevated 3-NT production in TH+ neurons at day 14 (Fig. 7B) compared to saline-treated *Ikbk2*$^{F/F}$ mice (Fig. 7A). In contrast, *hGfapcre/Ikbk2*$^{F/F}$ mice showed minimal 3-NT protein adducts in TH+ neurons in either saline (Fig. 7C) or MPTPp-treated mice at day 14 (Fig. 7D). Two-way ANOVA analysis of percent TH+ neurons expressing 3-NT reveal an effect of treatment ($F(2,19) = 7.44$, $p = 0.0041$)

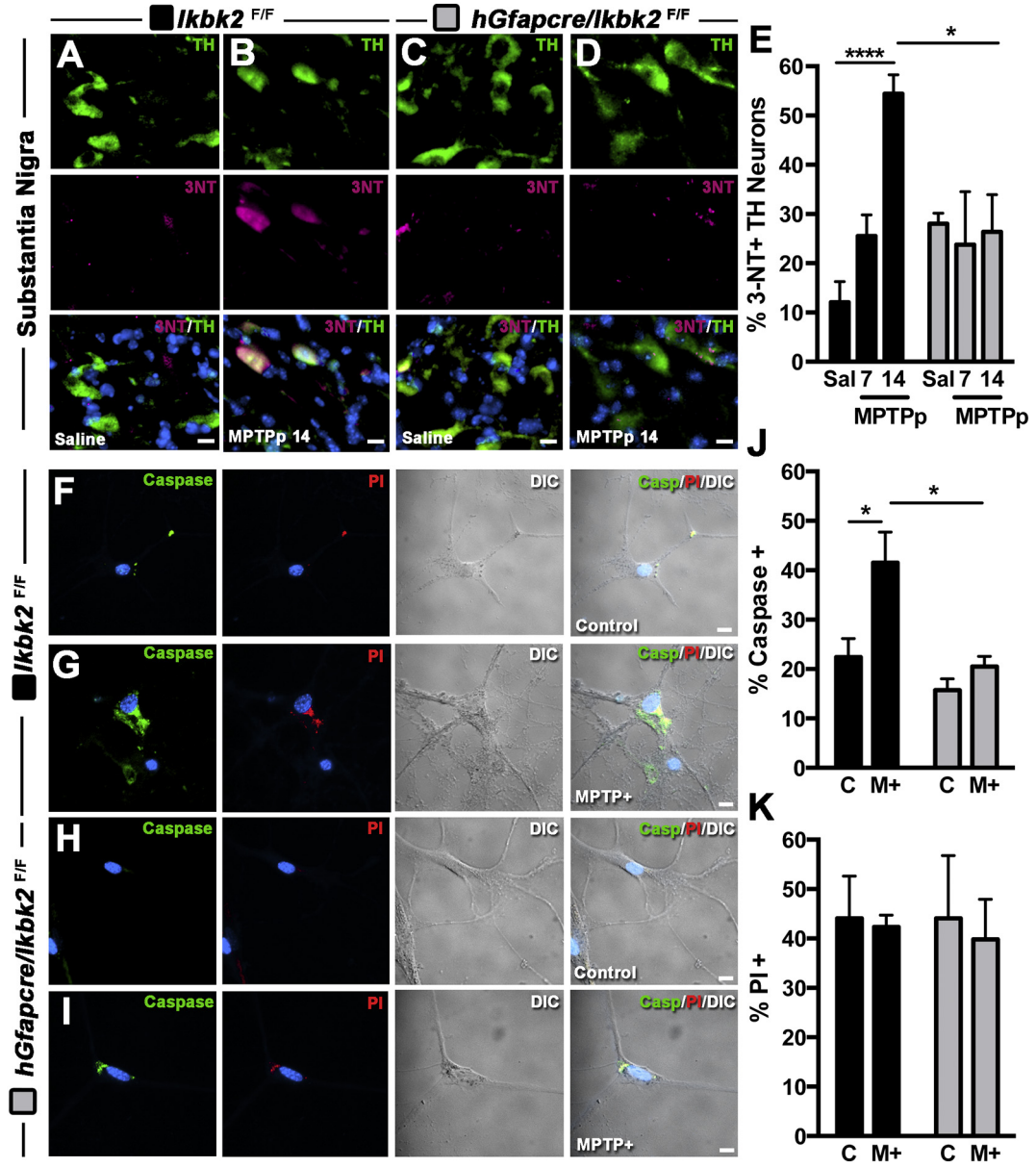

Fig. 7. Treatment with MPTPp results in the formation of 3-nitrotyrosine (3NT) adducts and activation of caspase 3 in dopaminergic neurons in *Ikbk2*$^{F/F}$ but not *hGfapcre/Ikbk2*$^{F/F}$ mice. A-E. Percent of 3NT expression in dopaminergic neurons was determined via immunofluorescence in the SN of *Ikbk2*$^{F/F}$ and *hGfapcre/Ikbk2*$^{F/F}$ mice treated with saline or MPTPp. Representative images of 3NT (magenta) and TH (green) co-localization counterstained with DAPI (cyan) in the SN of *Ikbk2*$^{F/F}$ (A,B) and *hGfapcre/Ikbk2*$^{F/F}$ (C, D) mice. E. Quantitative measurement of the percent of TH+ neurons within the SN of *Ikbk2*$^{F/F}$ (black bars) and *hGfapcre/Ikbk2*$^{F/F}$ (grey bars) mice positive for 3NT presented as mean percent ± SEM. F-K. Percent expression of caspase 3/7 and propidium iodide (PI) in cultured neurons co-cultured with astrocytes from *Ikbk2*$^{F/F}$ (black bars) and *hGfapcre/Ikbk2*$^{F/F}$ (grey bars) mice were determined via immunofluorescence. Representative images of caspase 3/7 (green) and PI (red) counterstained with DAPI (cyan) in cultured neurons co-cultured with astrocytes from *Ikbk2*$^{F/F}$ (F, G) and *hGfapcre/Ikbk2*$^{F/F}$ (H, I) mice exposed to vehicle or MPTP+. J. Quantitative measurement of the percent of caspase 3/7+ neurons presented as mean percent ± SEM. K. Quantitative measurement of the percent of PI+ neurons presented as mean percent ± SEM. All data were analyzed by two-way ANOVA with Tukey-Kramer post hoc test (* $p < 0.05$ and **** $p < 0.0001$). (For interpretation of the references to colour in this figure legend, the reader is referred to the web version of this article.)

with an interaction between treatment and genotype ($F(2,19) = 7.99$, $p = 0.003$; Fig. 7E). *Post-hoc* analysis revealed progressive increases in 3-NT in wild-type *Ikbk2*$^{F/F}$ mice following MPTPp treatment with significance from saline at day 14 ($p < 0.0001$), whereas *hGfapcre/Ikbk2*$^{F/F}$ mice showed no increases in the percent of TH+ neurons with 3-NT adducts following MPTPp treatment.

The function of IKK2 in astrocytes in modulating neuronal injury and apoptosis in the absence of direct MPP+ toxicity was investigated using live-cell fluorescence imaging of primary neurons. Neurons were exposed to glial conditioned medium (GCM) from *Ikbk2*$^{F/F}$ or *hGfapcre/Ikbk2*$^{F/F}$ astrocytes following treatment with MPTP and inflammatory cytokines (MPTP+/M+), as shown in representative fluorescence images of caspase 3/7, PI and differential interference contrast images (Fig. 7F-J; N = 6). Activation of caspase 3/7 as a measure of apoptosis, was rarely detected in control neurons exposed to GCM from saline-treated astrocytes from either *Ikbk2*$^{F/F}$ (Fig. 7F) or *hGfapcre/Ikbk2* $^{F/F}$ (Fig. 7H) mice. However, there were marked increase in caspase activation in neurons exposed to GCM from MPTP+-treated *Ikbk2*$^{F/F}$ astrocytes (Fig. 7G) but not MPTP+-treated *hGfapcre/Ikbk2*$^{F/F}$ astrocytes (Fig. 7I). Two-way ANOVA analysis of the percent of neurons expressing active caspase 3/7 showed an effect of treatment ($F(1,8) = 9.14$, $p = 0.017$) and genotype ($F(1,8) = 12.24$, $p = 0.0081$; Fig. 7J). *Post-*

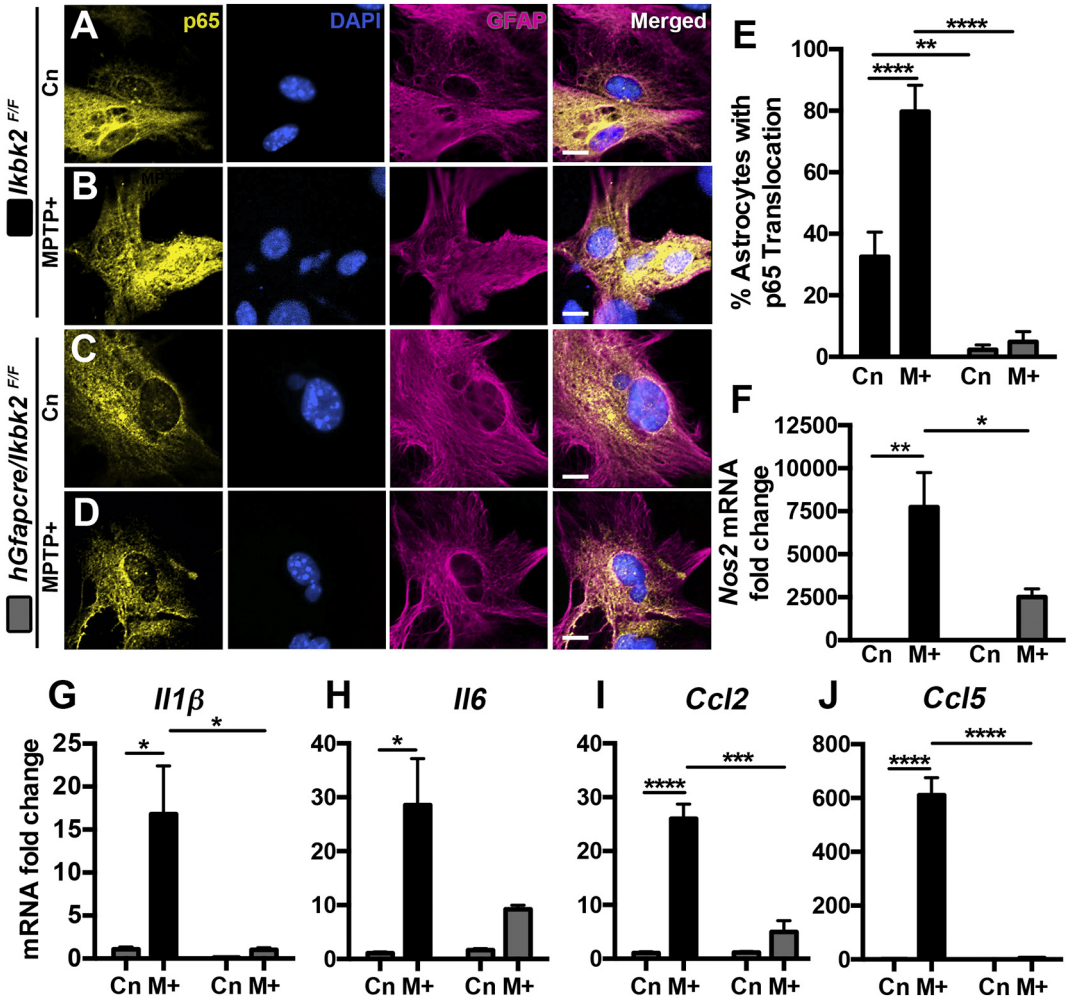

Fig. 8. Conditional deletion of *Ikbk2* in astrocytes prevents p65 translocation and suppresses activation of inflammatory genes in response to MPTP treatment. Primary cultures of astrocytes from *Ikbk2*$^{F/F}$ (black bars) and *hGfapcre/Ikbk2*$^{F/F}$ (grey bars) mice were treated with vehicle or MPTP and cytokines (M+) and assessed for p65 translocation via immunofluorescence or activation of inflammatory genes by qPCR. A-D. Representative images showing p65 (yellow) translocation in GFAP + (magenta) control or M+ treated astrocytes from *Ikbk2*$^{F/F}$ (A-B) and *hGfapcre/Ikbk2*$^{F/F}$ (C-D) mice counterstained with DAPI (cyan). E. Quantitative assessment of the % of astrocytes per image field with p65 translocation to the nucleus presented as mean percent ± SEM. F-J. mRNA fold change in inflammatory genes *Nos2* (F), *Il1β* (G), *Il6* (H), *Ccl2* (I), and *Ccl5* (J) in control or MPTP+ astrocytes from *Ikbk2*$^{F/F}$ (black bars) and *hGfapcre/Ikbk2*$^{F/F}$ (grey bars) mice presented as mean mRNA fold change ± SEM. All data was analyzed by two-way ANOVA with Tukey-Kramer post hoc test (* $p < 0.05$. ** $p < 0.01$, *** $p < 0.001$, and **** $p < 0.0001$). (For interpretation of the references to colour in this figure legend, the reader is referred to the web version of this article.)

hoc analysis revealed significant increases in caspase 3/7 only in neurons exposed to MPTP+ treated *Ikbk2*$^{F/F}$ astrocytes ($p = 0.037$) and that this increase was significantly different than the neuronal caspase 3/7% expression in neurons exposed to MPTP+-treated *hGfapcre/Ikbk2*$^{F/F}$ astrocytes ($p = 0.023$). Levels of PI were unchanged with treatment (Fig. 7K). These results indicate that treatment with MPTP leads to nitrosative stress and increased apoptosis in neurons that can be prevented by deletion of IKK2 in astrocytes.

3.7. Loss of IKK2 prevents MPTP-induced p65 translocation and activation of inflammatory genes in astrocytes

The previous data support that loss of IKK2 in astrocytes is neuroprotective both in vivo and in vitro, due at least in part to reductions in nitrosative stress and apoptosis in neurons. To identify specific factors within astrocytes regulating neuronal injury and apoptosis, we investigated translocation of p65 (Fig. 8A-E; N = 15–19) and pro-inflammatory gene expression (Fig. 8F-J; N = 3) in primary cultured astrocytes from *Ikbk2*$^{F/F}$ and *hGfapcre/Ikbk2*$^{F/F}$ mice exposed to MPTP +/M+ using immunofluorescence and qPCR, respectively. The number of astrocytes with p65 translocation to the nucleus, as shown in representative images, showed low nuclear expression in control *Ikbk2*$^{F/F}$ astrocytes (Fig. 8A) that markedly increased following 1-h exposure to MPTP+ (Fig. 8B). In contrast, astrocytes from *hGfapcre/Ikbk2*$^{F/F}$ mice had minimal nuclear p65 in control (Fig. 8C) that remained unchanged with MPTP+ treatment (Fig. 8D). Analysis of the percent of astrocytes with p65 translocation revealed an interaction of treatment and genotype ($F(1,63) = 11.69$; $p = 0.0011$; Fig. 8E). *Post-hoc* analysis revealed significant differences in p65 expression in control *Ikbk2*$^{F/F}$ and *hGfapcre/Ikbk2*$^{F/F}$ astrocytes ($p = 0.0071$), control *Ikbk2*$^{F/F}$ and MPTP+-treated *Ikbk2*$^{F/F}$ astrocytes ($p < 0.0001$), and MPTP +-treated *Ikbk2*$^{F/F}$ and *hGfapcre/Ikbk2*$^{F/F}$ astrocytes ($p < 0.0001$). Taken together, these data demonstrate that loss of IKK2 prevents even basal levels of p65 translocation to the nucleus and inhibits p65 translocation in response to an inflammatory stimulus.

Because nuclear translocation of p65 is necessary for NFκB-dependent transactivation of inflammatory genes, we examined the expression of multiple proinflammatory genes via qPCR in *Ikbk2*$^{F/F}$ astrocytes and in *hGfapcre/Ikbk2*$^{F/F}$ astrocytes (Fig. 8F-J). In wild type *Ikbk2*$^{F/F}$ astrocytes, exposure to MPTP+ resulted in significant increases in expression of *Nos2* ($p = 0.0032$; Fig. 8F), *Il1β* ($p = 0.018$; Fig. 8G), *Il6* ($p = 0.016$; Fig. 8H), *Ccl2* ($p < 0.0001$; Fig. 8I) and *Ccl5* ($p < 0.0001$;

Fig. 8J) that was minimal to absent in MPTP+ exposed *hGfapcre/Ikbk2$^{F/F}$* astrocytes. Analysis via two-way ANOVA revealed a significant interaction between treatment and genotype for all genes (*Nos2* $F(1,8) = 6.43$, $p = 0.035$; *Il1β* $F(1,8) = 6.95$, $p = 0.03$; *Ccl2* $F(1,7) = 38.24$, $p = 0.0005$; *Ccl5* $F(1,7) = 67.26$, $p < 0.0001$) except *Il6,* which only showed a significant effect of genotype ($F(1,7) = 12.85$, $p = 0.009$). This indicates that deletion of IKK2 in astrocytes inhibits the ability of astrocytes to express proinflammatory genes in response to treatment with MPTP and inflammatory cytokines.

4. Discussion

To understand the role of inflammatory activation of astrocytes in neurodegenerative disease, we generated an astrocyte-specific IKK2 knockout mouse (*hGfapcre/Ikbk2$^{F/F}$*), postulating that deletion of astrocytic IKK2 would protect mice against progressive neuronal loss when treated with MPTPp. To assess the extent and specificity of loss, the rate of IKK2 deletion was measured in primary astrocytes, microglia, and neurons from *hGfapcre/Ikbk2$^{F/F}$* and littermate controls (*Ikbk2$^{F/F}$*). The genomic frequency of recombination in astrocytes was ~ 70% (Fig. 1), which correlated with decreased protein levels as assessed by both western blotting and immunofluorescence (Figs. 1 and 2). Complete deletion of IKK2 was not observed, which is commonly seen with the use of Cre/loxP systems and often attributed to epigenetic modification of Cre expression (Kaufman et al., 2008). Other conditional Cre/loxP systems have reported even lower recombination rates, including 36% in a microglial-specific IKK2 knockout (Cho et al., 2008) and only 30 to 70% seen in other Gfap-Cre mouse models (Casper et al., 2007; Chow et al., 2008). Other factors that may have influenced the frequency of deletion could be the presence of low levels of microglia contamination in cell preparations, although studies from our laboratory often show 97% astrocyte purity in culture (Carbone et al., 2008). Another possibility is a clonal expansion of cells with incomplete deletion, which could account for the robust but partial deletion of IKK2 measured in immunopurified astrocytes, which could indicate a higher deletion rate in situ.

Cre-mediated deletion of IKK2 was found to be specific to astrocytes with no apparent loss measured in cultured microglia or striatal neurons (Fig. 2). Furthermore, this preservation of IKK2 was confirmed in vivo revealing that MAP2 positive neurons of the SNpc retained IKK2 (Fig. 2F-G). In vivo expression of IKK2 was not detectable in astrocytes or microglia in adult animals even in *Ikbk2$^{F/F}$* littermates (data not shown), consistent with other studies citing the same inability to detect glial expression of IKK2 in situ (Cho et al., 2008) and is most likely due to low constitutive expression Kaltschmidt et al., 2009). We were careful to confirm the specificity of deletion given the problems of the *hGFAP-cre* mouse showing expression in radial glial-derived neuronal populations prior to 3 months of age (Zhuo et al., 2001). We further confirmed this specificity by showing retention of IKK2 in the ST and SN neurons even though these neuronal populations are shown to be neuroepithelial derived and unlikely to express GFAP (Malatesta et al., 2003). Taken together, these data argue that we were successful in creating a conditional astrocyte-specific *Ikbk2* mouse and that *hGfapcre/Ikbk2$^{F/F}$* mice are a useful tool for elucidating the in vivo contribution of innate immune responses in astrocytes to neuroinflammation.

Other studies show that inhibition of NFκB is neuroprotective (Ghosh et al., 2007; Mondal et al., 2012; Hammond et al., 2018). However, these models employ the use of pharmacological inhibitors of NFκB and thus effects and mechanisms specific to neurons versus glial cells cannot be differentiated. Models employing specific deletion of IKK2 in astrocytes have shown to be neuroprotective (Cho et al., 2008; Brambilla et al., 2009; Dvoriantchikova et al., 2009) and evidence in cultured cells indicates that NFκB activation in astrocytes is important in MPTP-induced neuronal death (Carbone et al., 2008; Miller et al., 2011), but whether this translates to astrocytes in vivo in PD has not been proven. In this regard, our study clearly demonstrates an important role of for NFκB/IKK2-mediated astrocyte inflammation in neuronal injury in the MPTPp model of PD.

Astrocyte-specific IKK2 knockout mice (*hGfapcre/Ikbk2$^{F/F}$*) were treated with MPTP and probenecid to induce both loss of dopaminergic neurons and progressive inflammatory activation of glia. This dosing regimen has been previously published in our lab to produce more modest and progressive lesioning with MPTP that better recapitulates the slow, continuous loss of neurons seen in PD (De Miranda et al., 2013). *hGfapcre/Ikbk2$^{F/F}$* mice exposed to MPTP this model showed significant protection from both direct neurotoxicant induced SN dopaminergic neuronal loss as well as progressive inflammatory neuronal loss (Fig. 3). No significant loss of TH+ neurons was detected in *hGfapcre/Ikbk2$^{F/F}$* mice at day 7 and only 36% loss at day 14, compared to 45% and 60% loss in WT mice at day 7 and 14, respectively. This indicates that NFκB-dependent neuroinflammation in astrocytes has a vital role in not only progressive neuronal degeneration, but also in the initiation of MPTP neurotoxicity. This is consistent with experimental evidence where use of anti-inflammatory approaches prior to induction of neurotoxic injury to dopamine neurons was shown to be neuroprotective (Sugama et al., 2003; Sastre, 2010) but is in contrast to a study published by (Oeckl et al., 2012) where overexpression of astrocytic IKK2 did not enhance sensitivity to MPTP. However, Oeckl et al., 2012 employed an acute MPTP dosing strategy and showed enhanced neuroinflammation and loss of neurons even prior to dosing with high levels of constitutive neuroinflammation. Our data suggest that limiting innate immune inflammatory responses in astrocytes through the NFκB signaling pathway is directly neuroprotective.

In accordance with preservation of dopaminergic neurons, measures of neurobehavioral function in MPTPp-exposed mice indicated significant protection of *hGfapcre/Ikbk2$^{F/F}$* mice from reductions in locomotor activity (Fig. 4). This difference from littermate controls was most evident on day 7 of the treatment course. There appeared to be some functional recovery from these motor disturbances in all mice because, by day 14, *hGfapcre/Ikbk2$^{F/F}$* mice treated with MPTPp showed observable downward trends in both aforementioned parameters while treated *Ikbk2$^{F/F}$* mice showed partial recovery. The reversible nature of MPTP effects on hypokinesia is often observed after cessation of MPTP treatments (Sedelis et al., 2001; Miller et al., 2011), although other studies utilizing pharmacological inhibition of NFkB (Ghosh et al., 2007; Mondal et al., 2012) showed more persistent protection against changes in neurobehavior than measured in this study. These differences could be a factor that microglial and neuronal expression of NFκB remain unaltered in this model and thus may have important influences on MPTPp-induced alterations in locomotion.

The observed differences in neurobehavioral parameters between *Ikbk2$^{F/F}$* and *hGfapcre/Ikbk2$^{F/F}$* mice were not explainable by alterations in striatal catecholamines. Measurements of DA, DOPAC, and HVA were sharply reduced in striatal tissue all mice at both day 7 and day 14 even in the face of improved neurobehavior measures (Fig. 4). Other MPTP models have shown a similar disconnect between neurochemistry and neurobehavioral parameters (Dehmer et al., 2003; Miller et al., 2011; Mondal et al., 2012) that most likely reflects the insensitivity of catecholamine measurements to reflect subtle changes in brain environment and the ability of other systems to compensate for the changes in dopamine (Przedborski et al., 2000).

Despite lack of protection against MPTPp-induced loss of striatal catecholamines, *hGfapcre/Ikbk2$^{F/F}$* mice showed marked protection against dopaminergic nerve terminal loss (Fig. 3), striatal protein loss (Figs. 3 and 4) and MPTPp-induced peroxynitrite formation (Fig. 7) as compared to their wild-type *Ikbk2$^{F/F}$* littermates. VMAT and DAT are important in regulating intracellular and extracellular concentrations of DA with levels but functionally decline in PD due to protein loss and nitrosylation (German et al., 2015; Hammond et al., 2018). Additionally, peroxynitrite formed from NOS2 and NAPDH oxidase upregulation in glia impairs neuronal function further contributing to

neurobehavioral alterations (McCarty, 2006). Thus, preservation of these synaptic proteins likely contributes to preservation of locomotor reduction in *Ikk2* KO mice.

Loss of dopaminergic neurons is mediated by numerous factors including excitotoxicity, oxidant stress, mitochondrial dysregulation and direct cytotoxicity by glia-derived cytokines (Tansey and Goldberg, 2010; Durrenberger et al., 2014) that lead to neuronal apoptosis (Venderova and Park, 2012). In this model, we established that MPTPp treatment resulted in increased apoptotic gene expression in vivo (Fig. 6) that was reduced by deletion of IKK2 in astrocytes. These protections were unlikely caused by alterations in MPTP metabolism as alterations in MPTP metabolism are not shown when astrocyte IKK2 expression is altered (Oeckl et al., 2012). Because microarray of brain tissue is limited in power and specificity (Nisenbaum, 2002; Lewis and Cookson, 2012), we further confirmed protection of neuronal apoptosis through cell culture experiments (Fig. 7), confirming IKK2 deletion in astrocytes prevented caspase activation in neurons.

The decline in apoptotic gene expression was correlated with decreased neuronal nitrosative stress (Fig. 7), levels of gliosis (Fig. 5) and inflammatory gene expression (Figs. 6, 8 and Supp. Figs. 1, 2). IKK2 deletion in astrocytes only partly limited MPTPp-induced increases in astrocyte and microglia counts in the SN and was only fully protective against microglia increases in the ST. However, there was significant protection against astrocyte expression of inflammatory genes/proteins such as TNF, NOS2 and other cytokines and chemokines, most likely through suppression of p65 translocation (Fig. 8). Other studies of IKK2 suppression in astrocytes report similar results whereby astrocytosis remains unaltered while other parameters of glial inflammation including microgliosis are suppressed (More et al., 2013; Saggu et al., 2016; Douglass et al., 2017; Zhang et al., 2017), suggesting that IKK2 induces a reactive A1 inflammatory phenotype in astrocytes that subsequently enhances the reactivity of microglia (Liddelow et al., 2017). This finding may also be more broadly applicable to the role of reactive astrocytes in neurodegeneration, highlighted by studies demonstrating that an adeno-associated virus-based approach for inhibition of the Ca^{2+}/calmodulin-dependent phosphatase calcineurin (CN) and its target transcription factor, nuclear factor of activated T cells (NFAT4), in astrocytes prevents neuronal injury and Alzheimer's pathology in a mouse model of Alzheimer's disease (Sompol et al., 2017). The role of glial-glial communication in amplifying neuroinflammation (Saijo et al., 2009; Liddelow et al., 2017) underscores that targeting signaling pathways in astrocytes that regulate innate immune inflammatory responses can both reduce the severity of microgliosis and increase neuronal survival. We recently reported on this phenomenon, demonstrating that IKK2 in astrocytes directly regulates microglial reactivity through release of the chemokine, CCL2, which is required for neuronal injury in response to the neurotoxic metal, manganese (Popichak et al., 2018).

These data demonstrate that we were successful in generating mice with an astrocyte-specific deficiency in NFκB signaling. Utilizing this animal in a neurotoxin-based model of PD showed that inhibition of neuroinflammatory activation of astrocytes via NFκB protected against loss of dopaminergic neurons in the substantia nigra. The high degree of neuroprotection we observed in this model was associated with reductions in reactive gliosis and decreased production of glial-derived inflammatory mediators both in vivo and in vitro. This indicates that NFκB signaling in astrocytes is an important regulator of neuronal pathology in the MPTPp model of PD and also suggests that this and related pathways regulating neuroinflammation and glial reactivity could be important therapeutic targets for disease modification.

Acknowledgments

The authors would like to thank Michael Karin for providing the floxed-Ikbk2 mouse and other members of the Tjalkens lab (Jim Miller and Briana De Miranda) who supported completion of this study. This work was funded by National Institutes of Health grant 5R01ES024183 (RBT).

Appendix A. Supplementary data

Supplementary data to this article can be found online at https://doi.org/10.1016/j.nbd.2019.02.020.

References

Aschner, M., Kimelberg, H.K., 1991. The use of astrocytes in culture as model systems for evaluating neurotoxic-induced-injury. Neurotoxicology 12, 505–517.
Bonizzi, G., Karin, M., 2004. The two NF-κB activation pathways and their role in innate and adaptive immunity. Trends Immunol. 25, 280–288.
Brambilla, R., 2005. Inhibition of astroglial nuclear factor B reduces inflammation and improves functional recovery after spinal cord injury. J. Exp. Med. 202, 145–156.
Brambilla, R., Persaud, T., Hu, X., Karmally, S., Shestopalov, V.I., Dvoriantchikova, G., Ivanov, D., Nathanson, L., Barnum, S.R., Bethea, J.R., 2009. Transgenic inhibition of Astroglial NF- B improves functional outcome in experimental autoimmune encephalomyelitis by suppressing chronic central nervous system inflammation. J. Immunol. 182, 2628–2640.
Burda, J.E., Sofroniew, M.V., 2014. Reactive gliosis and the multicellular response to CNS damage and disease. Neuron 81, 229–248.
Carbone, D.L., Popichak, K.A., Moreno, J.A., Safe, S., Tjalkens, R.B., 2008. Suppression of 1-Methyl-4-phenyl-1,2,3,6-tetrahydropyridine-induced nitric-oxide synthase 2 expression in astrocytes by a novel Diindolylmethane Analog protects striatal neurons against apoptosis. Mol. Pharmacol. 75, 35–43.
Casper, K.B., McCarthy, K.D., 2006. GFAP-positive progenitor cells produce neurons and oligodendrocytes throughout the CNS. Mol. Cell. Neurosci. 31, 676–684.
Casper, K.B., Jones, K., McCarthy, K.D., 2007. Characterization of astrocyte-specific conditional knockouts. Genesis 45, 292–299.
Chen, P.C., Vargas, M.R., Pani, A.K., Smeyne, R.J., Johnson, D.A., Kan, Y.W., Johnson, J.A., 2009. Nrf2-mediated neuroprotection in the MPTP mouse model of Parkinson's disease: critical role for the astrocyte. Proc. Natl. Acad. Sci. USA 106, 2933–2938.
Cheng, S., Hou, J., Zhang, C., Xu, C., Wang, L., Zou, X., Yu, H., Shi, Y., Yin, Z., Chen, G., 2015. MInocycline reduces neuroinflammation but does not ameliorate neuronal loss in a mouse model of neurodegeneration. Sci. Rep. 5, 10535.
Cho, I.H., Hong, J., Suh, E.C., Kim, J.H., Lee, H., Lee, J.E., Lee, S., Kim, C.H., Kim, D.W., Jo, E.K., Lee, K.E., Karin, M., Lee, S.J., 2008. Role of microglial IKK in kainic acid-induced hippocampal neuronal cell death. Brain 131, 3019–3033.
Chow, L.M.L., Zhang, J., Baker, S.J., 2008. Inducible Cre recombinase activity in mouse mature astrocytes and adult neural precursor cells. Transgenic Res. 17, 919–928.
Da Wei Huang, Sherman B.T., Lempicki, R.A., 2009. Systematic and integrative analysis of large gene lists using DAVID bioinformatics resources. Nat. Protoc. 4, 44–57.
Damier, P., Hirsch, E.C., Zhang, P., Agid, Y., Javoy-Agid, F., 1993. Glutathione peroxidase, glial cells and Parkinson's disease. Neuroscience 52, 1–6.
De Miranda, B.R., Miller, J.A., Hansen, R.J., Lunghofer, P.J., Safe, S., Gustafson, D.L., Colagiovanni, D., Tjalkens, R.B., 2013. Neuroprotective efficacy and pharmacokinetic behavior of novel anti-inflammatory Para-phenyl substituted Diindolylmethanes in a mouse model of Parkinson's disease. J. Pharmacol. Exp. Ther. 345, 125–138.
Dehmer, T., Lindenau, J., Haid, S., Dichgans, J., Schulz, J.B., 2000. Deficiency of inducible nitric oxide synthase protects against MPTP toxicity in vivo. J. Neurochem. 74, 2213–2216.
Dehmer, T., Heneka, M.T., Sastre, M., Dichgans, J., Schulz, J.B., 2003. Protection by pioglitazone in the MPTP model of Parkinson's disease correlates with IκBα induction and block of NFκB and iNOS activation. J. Neurochem. 88, 494–501.
Douglass, J.D., Dorfman, M.D., Fasnacht, R., Shaffer, L.D., Thaler, J.P., 2017. Astrocyte IKKbeta/NF-kappaB signaling is required for diet-induced obesity and hypothalamic inflammation. Molecular Metabolism 6, 366–373.
Durrenberger, P.F., Fernando, F.S., Kashefi, S.N., Bonnert, T.P., Seilhean, D., Nait-Oumesmar, B., Schmitt, A., Gebicke-Haerter, P.J., Falkai, P., Grünblatt, E., Palkovits, M., Arzberger, T., Kretzschmar, H., Dexter, D.T., Reynolds, R., 2014. Common mechanisms in neurodegeneration and neuroinflammation: a BrainNet Europe gene expression microarray study. J. Neural Transm. 122, 1055–1068.
Dvoriantchikova, G., Barakat, D., Brambilla, R., Agudelo, C., Hernandez, E., Bethea, J.R., Shestopalov, V.I., Ivanov, D., 2009. Inactivation of astroglial NF-κB promotes survival of retinal neurons following ischemic injury. Eur. J. Neurosci. 30, 175–185.
Dzamko, N., Geczy, C.L., Halliday, G.M., 2015. Inflammation is genetically implicated in Parkinson's disease. Neuroscience 302, 89–102.
Frank-Cannon, T.C., Alto, L.T., McAlpine, F.E., Tansey, M.G., 2009. Does neuroinflammation fan the flame in neurodegenerative diseases? Mol. Neurodegener. 4, 47.
Fredriksson, A., Plaznik, A., Sundström, E., Jonsson, G., Archer, T., 1990. MPTP-induced hypoactivity in mice: reversal by L-dopa. Pharmacol. Toxicol. 67, 295–301.
German, C.L., Baladi, M.G., McFadden, L.M., Hanson, G.R., Fleckenstein, A.E., Daws, L.C., 2015. Regulation of the dopamine and vesicular monoamine transporters: pharmacological targets and implications for disease. Pharmacol. Rev. 67, 1005–1024.
Ghosh, A., Roy, A., Liu, X., Kordower, J.H., Mufson, E.J., Hartley, D.M., Ghosh, S., Mosley, R.L., Gendelman, H.E., Pahan, K., 2007. Selective inhibition of NF-κB activation prevents dopaminergic neuronal loss in a mouse model of Parkinson's disease. Proc. Natl. Acad. Sci. U. S. A. 104, 18754–18759.
Glass, C.K., Saijo, K., Winner, B., Marchetto, M.C., Gage, F.H., 2010. Mechanisms underlying inflammation in Neurodegeneration. Cell 140, 918–934.
Gordon, R.R., Hogan, C.E.C., Neal, M.L.M., Anantharam, V.V., Kanthasamy, A.G.A.,

Kanthasamy, A.A., 2011. A simple magnetic separation method for high-yield isolation of pure primary microglia. J. Neurosci. Methods 194, 287–296.
Grilli, M., Memo, M., 1999. Nuclear factor-κB/Rel proteins. Biochem. Pharmacol. 57, 1–7.
Hammond, S.L., Popichak, K.A., Li, X., Hunt, L.G., Richman, E.H., Damale, P.U., Chong, E.K.P., Backos, D.S., Safe, S., Tjalkens, R.B., 2018. The Nurr1 Ligand,1,1-bis(3'-Indolyl)-1-(p-Chlorophenyl)methane, modulates glial reactivity and is Neuroprotective in MPTP-induced parkinsonism. J. Pharmacol. Exp. Ther. 365, 636–651.
Herrmann, O., Baumann, B., de Lorenzi, R., Muhammad, S., Zhang, W., Kleesiek, J., Malfertheiner, M., Köhrmann, M., Potrovita, I., Maegele, I., Beyer, C., Burke, J.R., Hasan, M.T., Bujard, H., Wirth, T., Pasparakis, M., Schwaninger, M., 2005. IKK mediates ischemia-induced neuronal death. Nat. Med. 11, 1322–1329.
Hirsch, E.C., Hunot, S., 2009. Neuroinflammation in Parkinson's disease: a target for neuroprotection? Lancet Neurol. 8, 382–397.
Huang, D.W., Sherman, B.T., 2009. Bioinformatics enrichment tools: paths toward the comprehensive functional analysis of large gene lists. Nucleic Acid Res. 37, 1–13.
Hunot, S., Brugg, B., Ricard, D., Michel, P.P., Muriel, M.-P., Ruberg, M., Faucheux, B.A., Agid, Y., Hirsch, E.C., 1997. Nuclear translocation of NF-κB is increased in dopaminergic neurons of patients with Parkinson disease. Proc. Natl. Acad. Sci. U. S. A. 95, 7531–7536.
Karin, M., 1999. The role of the IkB kinase (IKK) complex. Oncogene 1–8.
Karin, M., 2005. Inflammation-activated protein kinases as targets for drug development. Proc. Am. Thorac. Soc. 2, 386–390.
Kaufman, W.L., Kocman, I., Agrawal, V., Rahn, H.P., Besser, D., Gossen, M., 2008. Homogeneity and persistence of transgene expression by omitting antibiotic selection in cell line isolation. Nucleic Acids Res. 36, e111.
Kirkley, K.S., Popichak, K.A., Afzali, M.F., Legare, M.E., Tjalkens, R.B., 2017a. Microglia amplify inflammatory activation of astrocytes in manganese neurotoxicity. J. Neuroinflammation 14, 1–18.
Kirkley, K.S., Walton, K.D., Duncan, C., Tjalkens, R.B., 2017b. Spontaneous development of cutaneous squamous cell carcinoma in mice with cell-specific deletion of inhibitor of kappaB kinase 2. Comp. Med. 67, 407–415.
Lewis, P.A., Cookson, M.R., 2012. Gene expression in the Parkinson's disease brain. Brain Res. Bull. 88, 302–312.
Li, Z.-W., Omori, S.A., Labuda, T., Karin, M., Rickert, R.C., 2003. IKK beta is required for peripheral B cell survival and proliferation. J. Immunol. 170, 4630–4637.
Liddelow, S.A., Guttenplan, K.A., Clarke, L.E., Bennett, F.C., Bohlen, C.J., Schirmer, L., Bennett, M.L., Munch, A.E., Chung, W.S., Peterson, T.C., Wilton, D.K., Frouin, A., Napier, B.A., Panicker, N., Kumar, M., Buckwalter, M.S., Rowitch, D.H., Dawson, V.L., Dawson, T.M., Stevens, B., Barres, B.A., 2017. Neurotoxic reactive astrocytes are induced by activated microglia. Nature. 541, 481–487.
Liu, X.X., Sullivan, K.A.K., Madl, J.E.J., Legare, M.M., Tjalkens, R.B.R., 2006. Manganese-induced neurotoxicity: the role of astroglial-derived nitric oxide in striatal interneuron degeneration. Toxicol. Sci. 91, 521–531.
Malatesta, P., Hack, M.A., Hartfuss, E., Kettenmann, H., Klinkert, W., Kirchhoff, F., Götz, M., 2003. Neuronal or glial progeny: regional differences in radial glia fate. Neuron 37, 751–764.
Mattson, M.P., Camandola, S., 2001. NF-κB in neuronal plasticity and neurodegenerative disorders. J. Clin. Invest. 107, 247–254.
McCarty, M.F., 2006. Down-regulation of microglial activation may represent a practical strategy for combating neurodegenerative disorders. Med. Hypotheses 67, 251–269.
Mettang, M., Reichel, S.N., Lattke, M., Palmer, A., Abaei, A., Rasche, V., Huber-Lang, M., Baumann, B., Wirth, T., 2018. IKK2/NF-κB signaling protects neurons after traumatic brain injury. FASEB J. 32, 1916–1932.
Miller, J.A., Trout, B.R., Sullivan, K.A., Bialecki, R.A., Roberts, R.A., Tjalkens, R.B., 2011. Low-dose 1-methyl-4-phenyl-1,2,3,6-tetrahydropyridine causes inflammatory activation of astrocytes in nuclear factor-κB reporter mice prior to loss of dopaminergic neurons. J. Neurosci. Res. 89, 406–417.
Mondal, S., Roy, A., Jana, A., Ghosh, S., Kordower, J.H., Pahan, K., 2012. Testing NF-κB-based therapy in Hemiparkinsonian monkeys. J. NeuroImmune. Pharm. 7, 544–556.
More, S.V., Kumar, H., Kim, I.S., Song, S.-Y., Choi, D.-K., 2013. Cellular and molecular mediators of neuroinflammation in the pathogenesis of Parkinson's disease. Mediat. Inflamm. 2013, 1–12.
Moreno, J.A., Sullivan, K.A., Carbone, D.L., Hanneman, W.H., Tjalkens, R.B., 2008. Manganese potentiates nuclear factor-kappaB-dependent expression of nitric oxide synthase 2 in astrocytes by activating soluble guanylate cyclase and extracellular responsive kinase signaling pathways. J. Neurosci. Res. 86, 2028–2038.
Moreno, J.A., Yeomans, E.C., Streifel, K.M., Brattin, B.L., Taylor, R.J., Tjalkens, R.B., 2009. Age-dependent susceptibility to manganese-induced neurological dysfunction. Toxicol. Sci. 112, 394–404.
Nagatsu, T., Sawada, M., 2005. Inflammatory process in Parkinson's disease: role for cytokines. Curr. Pharm. Des. 11, 999–1016.
Neal, M., Richardson, J.R., 2018. Epigenetic regulation of astrocyte function in neuroinflammation and neurodegeneration. Biochim. Biophys. Acta 1864, 432–443.
Nisenbaum, L.K., 2002. The ultimate chip shot: can microarray technology deliver for neuroscience? Genes Brain Behav. 1, 27–34.
Oeckl, P., Lattke, M., Wirth, T., Baumann, B., Ferger, B., 2012. Astrocyte-specific IKK2 activation in mice is sufficient to induce neuroinflammation but does not increase susceptibility to MPTP. Neurobiol. Dis. 48, 481–487.
Ouchi, Y., Yagi, S., Yokokura, M., Sakamoto, M., 2009. Neuroinflammation in the living brain of Parkinson's disease. Parkinsonism Relat. Disord. 15 (Suppl. 3), S200–S204.
Perez, F.A., Palmiter, R.D., 2005. Parkin-deficient mice are not a robust model of parkinsonism. Proc. Natl. Acad. Sci. U. S. A. 102, 2174–2179.
Popichak, K.A., Afzali, M.F., Kirkley, K.S., Tjalkens, R.B., 2018. Glial-neuronal signaling mechanisms underlying the neuroinflammatory effects of manganese. J. Neuroinflammation 15, 324.
Przedborski, S., Jackson-Lewis, V., Djaldetti, R., Liberatore, G., Vila, M., Vukosavic, S., Almer, G., 2000. The parkinsonian toxin MPTP: action and mechanism. Restor. Neurol. Neurosci. 16, 135–142.
Saggu, R., Schumacher, T., Gerich, F., Rakers, C., Tai, K., Delekate, A., Petzold, G.C., 2016. Astroglial NF-kB contributes to white matter damage and cognitive impairment in a mouse model of vascular dementia. Acta Neuropathol. Commun. 4, 1–76.
Saijo, K., Winner, B., Carson, C.T., Collier, J.G., Boyer, L., Rosenfeld, M.G., Gage, F.H., Glass, C.K., 2009. A Nurr1/CoREST pathway in microglia and astrocytes protects dopaminergic neurons from inflammation-induced death. Cell 137, 47–59.
Sastre, M., 2010. NSAIDs: how they work and their prospects as therapeutics in Alzheimer's disease. Front Ag Neurosci 2, 1–6.
Sedelis, M., Schwarting, R.K.W., Huston, J.P., 2001. Behavioral phenotyping of the MPTP mouse model of Parkinson's disease. Behav. Brain Res. 125, 109–125.
Sompol, P., Furman, J.L., Pleiss, M.M., Kraner, S.D., Artiushin, I.A., Batten, S.R., Quintero, J.E., Simmerman, L.A., Beckett, T.L., Lovell, M.A., Murphy, M.P., Gerhardt, G.A., Norris, C.M., 2017. Calcineurin/NFAT Signaling in activated astrocytes drives network Hyperexcitability in Abeta-bearing mice. J. Neurosci. 37, 6132–6148.
Streifel, K.M., Moreno, J.A., Hanneman, W.H., Legare, M.E., Tjalkens, R.B., 2012. Gene deletion of nos2 protects against manganese-induced neurological dysfunction in juvenile mice. Toxicol. Sci. 126, 183–192.
Sugama, S., Yang, L., Cho, B.P., DeGiorgio, L.A., Lorenzl, S., Albers, D.S., Beal, M.F., Volpe, B.T., Joh, T.H., 2003. Age-related microglial activation in 1-methyl-4-phenyl-1, 2, 3, 6-tetrahydropyridine (MPTP)-induced dopaminergic neurodegeneration in C57BL/6 mice. Brain Res. 964, 288–294.
Tansey, M.G., Goldberg, M.S., 2010. Neuroinflammation in Parkinson's disease: its role in neuronal death and implications for therapeutic intervention. Neurobiol. Dis. 37, 510–518.
Tusher, V., Tibshirani, R., Chu, G., 2001. SAM significance analysis of Microarraysapplied to transcriptional responses to ionizing radiation. Proc. Natl. Acad. Sci. U. S. A. 98, 5116–5121.
Van Loo, G., de Lorenzi, R., Schmidt, H., Huth, M., Mildner, A., Schmidt-Supprian, M., Lassmann, H., Prinz, M.R., Pasparakis, M., 2006. Inhibition of transcription factor NF-κB in the central nervous system ameliorates autoimmune encephalomyelitis in mice. Nat. Immunol. 7, 954–961.
Venderova, K., Park, D.S., 2012. Programmed cell death in Parkinson's disease. Cold Spring Harb Perspect Med 2, a009365.
Zhang, Y., Reichel, J.M., Han, C., Zuniga-Hertz, J.P., Cai, D., 2017. Astrocytic process plasticity and IKKbeta;/NF-&kappaB in central control of blood glucose, blood pressure, and body weight. Cell Metab. 25, 1091–1102.
Zhuo, L., Theis, M., Alvarez-Maya, I., Brenner, M., Willecke, K., Messing, A., 2001. hGFAP-cre transgenic mice for manipulation of glial and neuronal function in vivo. Genesis 31, 85–94.